



## Research paper

# Design, synthesis and bioactivity study of N-salicyloyl tryptamine derivatives as multifunctional agents for the treatment of neuroinflammation

Xiaohong Fan <sup>a,1</sup>, Junfang Li <sup>a,1</sup>, Xuemei Deng <sup>a,1</sup>, Yingmei Lu <sup>a</sup>, Yiyue Feng <sup>a</sup>, Shumeng Ma <sup>a</sup>, Huaixiu Wen <sup>c</sup>, Quanyi Zhao <sup>a</sup>, Wen Tan <sup>a</sup>, Tao Shi <sup>a,\*\*</sup>, Zhen Wang <sup>a,b,\*</sup>

<sup>a</sup> School of Pharmacy, Lanzhou University, Lanzhou, 730000, China

<sup>b</sup> State Key Laboratory of Applied Organic Chemistry, College of Chemistry and Chemical Engineering, Lanzhou University, Lanzhou, 730000, China

<sup>c</sup> Key Laboratory of Tibetan Medicine Research, Northwest Institute of Plateau Biology, Chinese Academy of Sciences, Xining, 810000, China

## ARTICLE INFO

## Article history:

Received 17 January 2020

Received in revised form

3 March 2020

Accepted 7 March 2020

Available online 9 March 2020

## Keywords:

Combination principle

N-salicyloyl tryptamine

Neurodegenerative diseases

Neuroinflammation

Multifunction

## ABSTRACT

Because of the complex etiology in neuroinflammatory process, the design of multifunctional agents is a potent strategy to cure neuroinflammatory diseases including AD and PD. Herein, based on the combination principles, 23 of N-salicyloyl tryptamine derivatives as multifunctional agents were designed and their new application for anti-neuroinflammation was disclosed. In cyclooxygenase assay, two compounds **3** and **16** displayed extremely preferable COX-2 inhibition than N-salicyloyl tryptamine. In LPS-induced C6 and BV2 cell models, some compounds decreased the production of proinflammatory mediators NO, PGE<sub>2</sub>, TNF- $\alpha$ , iNOS, COX-2 and ROS, while increased the production of IL-10. Among them, compound **3** and **16** showed approximately six-fold better inhibition on nitric oxide production than N-salicyloyl tryptamine in C6. Besides, compounds **3**, **13** and **16** attenuated the activation of BV2 and C6 cells. More importantly, in vivo, compounds **3** and **16** reduced GFAP and Iba-1 levels in the hippocampus, and displayed neuroprotection in Nissl staining. Besides, both compounds **3** and **16** had high safety (LD<sub>50</sub> > 1000 mg/kg). Longer plasma half-life of compounds **3** and **16** than melatonin supported combination strategy. All these results demonstrated that N-salicyloyl tryptamine derivatives are potential anti-neuroinflammation agents for the treatment of neurodegenerative disorder.

© 2020 Elsevier Masson SAS. All rights reserved.

## 1. Introduction

Neuroinflammation is an important defense mechanism against injury toxins, but persistent neuroinflammation can result in neuronal death and ultimately contribute to neurodegeneration, such as Alzheimer's (AD) or Parkinson's (PD) diseases [1]. It is characterized by activation of resident immune cells (microglia and astrocytes), which cause production of proinflammatory cytokines and neuronal damage [2–7]. Recently, an approved drug for the treatment of Alzheimer's diseases, GV-971, does takes effect partially due to inhibition of neuroinflammation [8]. This indicates

that development of anti-neuroinflammatory drugs for the treatment of neurodegenerative diseases is promising [9]. However, due to extremely complex and dynamic process which resembles a well-orchestrated symphony of neuroinflammation, many agents modulating at one process could only enable a palliative treatment instead of definitively curing [10]. Therefore, seeking the multifunctional candidates is an imperative strategy of designing anti-neuroinflammation agents.

Melatonin, a versatile endogenous hormone, has been proved to prevent neuroinflammation by inhibiting activation of microglia and astrocyte [11–14]. Furthermore, high drug-able profiles (high lipophilicity and easy permeability through the blood-brain barrier), exalt its application for neuroinflammatory treatment [15–17]. However, it exerts poor pharmacokinetic properties, such as a short plasma half-life (~30 min), which limits its use for neuroinflammation [18]. Thus, rational modifications based on the template of melatonin were conducted (Scheme 1) [19]. Besides, salicylic acid derivatives have been reported to alleviate

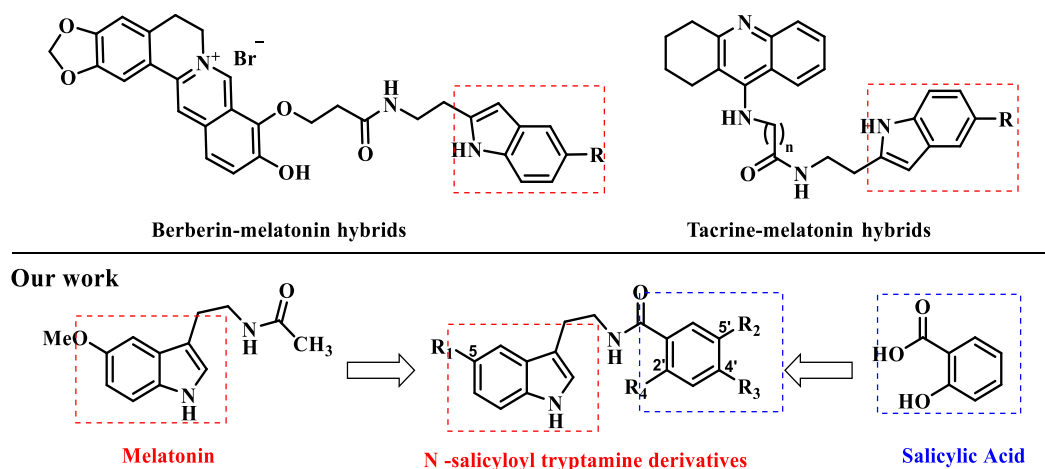
\* Corresponding author. School of Pharmacy, Lanzhou University, Lanzhou, 730000, China.

\*\* Corresponding author.

E-mail addresses: [shit18@lzu.edu.cn](mailto:shit18@lzu.edu.cn) (T. Shi), [zhenw@lzu.edu.cn](mailto:zhenw@lzu.edu.cn) (Z. Wang).

<sup>1</sup> These authors contributed equally to the work.

### Previous work



**Scheme 1.** Design of the target compounds.

neuroinflammation [20–27]. The mechanism may involve targeting COX, a therapeutic target for treating neuroinflammation [28–35]. Nevertheless, the lack of repair capacity on damaged neuron, limited exposure to brains and varying degrees of side effects narrow their application on long-term clinical use [29,36,37]. Thus, it is worth to combine salicylic acid derivatives with melatonin to develop multifunctional molecules as anti-neuroinflammatory agents.

Based on above findings, we reported a series of N-salicyloyl tryptamine derivatives with multifunctional properties including radicals scavenging, COX inhibition, attenuating activation of glial cells, and attenuating neuronal damage (Scheme 1). Although N-salicyloyl tryptamine was applied as anticonvulsant agents or anti-inflammatory agents in RAW264.7 model, its new application as anti-neuroinflammatory agents has not been reported [38–44]. To develop more potent anti-neuroinflammatory activities than the parent compound N-salicyloyl tryptamine, two kinds of derivatives which had different substituents (hydroxyl, amine) in C2' were synthesized. After the introduction of different substituents with various electronic and steric properties in C5, C4', C5' position, the structure-activity relationship study on cyclooxygenase inhibition assay was conducted, followed by LPS-induced glial cells model and LPS-induced neuroinflammatory model of mice. Taken together, all data suggest that the strategy of combining tryptamine derivatives and salicylic acid derivatives provides a new sight of designing multi-functional candidates for neuroinflammation related neurodegenerative diseases.

## 2. Results and discussion

### 2.1. Synthesis

Well-established methodology was utilized in the synthesis of N-salicyloyl tryptamine derivatives as indicated in Scheme 2. In detail, target compounds were obtained by condensation reaction using salicylic acid derivatives and tryptamine derivatives in the presence of EDCl, HOBT and triethylamine [45]. All the compounds were synthesized in near quantitative yields (70%–90%), characterized by NMR and mass spectrometry, and analyzed by HPLC suggesting a minimum purity of 95.0%.

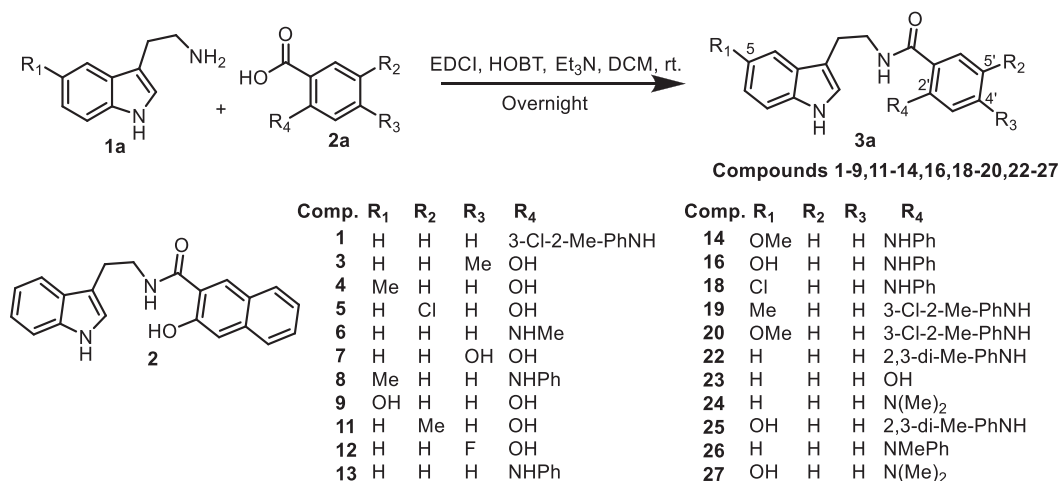
<sup>a</sup>Compounds **1** [46], **2** [46], **3** [50], **4** [51], **5** [50], **6** [48], **8** [46], **9** [44], **11** [46], **12** [46], **13** [46], **14** [46], **18** [46], **22** [49], **23** [39], **24** [47]

have been previously described. Except for these compounds mentioned above, compounds **7**, **16**, **19**, **20**, **25**, **26**, **27** were not reported before.

### 2.2. COX inhibition assay and structure-activity relationship study

To confirm the COX inhibitory effects of all synthesized compounds, COX inhibitor screening assay was performed using commercial assay kits and salicylic acid as a control. As shown in Table 1, the compounds exhibited differently inhibitory effects on the COX with IC<sub>50</sub> values ranging from 0.50 to more than over 40 μM. Among them, 15 compounds showed extremely better inhibition on COX-2 than salicylic acid. Additionally, some compounds had slight selectivity on COX-2. The primary structure-activity relationships in C5, C2' and other positions in the phenyl ring of salicylic acid moiety were reported as follows:

- i) When R<sub>4</sub> in C2' was a hydroxyl, the activity was determined by comprehensive factors of substituents in C5 and other positions of salicylic acid moiety. Firstly, in C5 position, the COX-2 inhibitory potency order was OH > Me and H (Compounds **9** > **4** and **23**). Compared to C5 unsubstituted parent compound **23** (IC<sub>50</sub> > 40 μM), a dramatic increase in activity was seen by the introduction of OH in C5 (compound **9**, IC<sub>50</sub> = 0.80 ± 0.35 μM) which was the third-best one on COX-2 inhibition. Secondly, in C4' position, the COX-2 inhibitory potency order was Me > OH > F and H (Compounds **3** > **7** > **12** and **23**), suggesting that introduction of the electron-donating group in C4' achieved an improved activity. In contrast, in C5' position, the COX-2 inhibitory potency order for these compounds was Cl > Me and H (Compound **5** > **11** and **23**), indicating that introduction of electron-withdrawing group in C5' was beneficial to activity improvement. Interestingly, when the phenyl ring (compound **23**, IC<sub>50</sub> > 40 μM) was changed to naphthyl ring (compound **2**, IC<sub>50</sub> = 2.18 ± 0.48 μM), a significantly improved COX-2 inhibitory activity was observed, identifying that enlarged conjugate plane was favorable to COX-2 inhibition.
- ii) When R<sub>4</sub> in C2' was an amine, the SAR study in C5 was conducted. When R<sub>4</sub> was NHPH, the COX-2 inhibitory potency order for these compounds was OH > Cl > Me > H > OMe. Namely, compound **16** was the best one on COX-2 inhibition (IC<sub>50</sub> = 0.50 ± 0.10 μM), followed by compounds **18**, **8**, **13**, **14**. For

Scheme 2. Synthesis of N-salicyloyl tryptamine derivatives.<sup>a</sup>Table 1  
Inhibitory effects of compounds against COX-2 and COX-1.

Comp.	R <sub>1</sub>	R <sub>2</sub>	R <sub>3</sub>	R <sub>4</sub>	hCOX-2 IC <sub>50</sub> (μM) ± SD <sup>a</sup>	hCOX-1 IC <sub>50</sub> (μM) ± SD <sup>a</sup>	SI <sup>b</sup>
1	H	H	H	3-Cl-2-Me-PhNH	14.54 ± 2.12	—	—
2	—	—	—	—	2.18 ± 0.48	39.21 ± 2.18	17.98
3	H	H	Me	OH	4.16 ± 0.43	16.44 ± 1.43	3.95
4	Me	H	H	OH	>40	>40	—
5	H	Cl	H	OH	10.37 ± 1.59	>40	—
6	H	H	H	NHMe	>40	>40	—
7	H	H	OH	OH	25.00 ± 5.64	>40	—
8	Me	H	H	NHPh	1.47 ± 0.47	27.05 ± 4.46	18.40
9	OH	H	H	OH	0.80 ± 0.35	1.74 ± 0.61	2.18
11	H	Me	H	OH	>40	>40	—
12	H	H	F	OH	>40	>40	—
13	H	H	H	NHPh	2.62 ± 0.98	0.47 ± 0.01	0.18
14	OMe	H	H	NHPh	2.76 ± 0.64	38.64 ± 5.89	14.00
16	OH	H	H	NHPh	0.50 ± 0.10	0.38 ± 0.05	0.76
18	Cl	H	H	NHPh	0.58 ± 0.19	1.34 ± 0.25	2.31
19	Me	H	H	3-Cl-2-Me-PhNH	9.72 ± 2.54	—	—
20	OMe	H	H	3-Cl-2-Me-PhNH	>40	—	—
22	H	H	H	2,3-di-Me-PhNH	2.31 ± 0.22	—	—
23	H	H	H	OH	>40	—	—
24	H	H	H	N(Me) <sub>2</sub>	>40	—	—
25	OH	H	H	2,3-di-Me-PhNH	1.40 ± 0.13	—	—
26	H	H	H	NMePh	>40	—	—
27	OH	H	H	N(Me) <sub>2</sub>	0.57 ± 0.13	—	—
BHA <sup>c</sup>	—	—	—	—	>40	>40	—

<sup>a</sup> IC<sub>50</sub> (μM), the concentrations of compounds producing 50% inhibition of human recombinant COX-1 and COX-2 in vitro. The IC<sub>50</sub> values were determined by a dose-response inhibition curve with GraphPad PRISM. All assays were performed in triplicate with data pooled from at least three independent experiments.

<sup>b</sup> In vitro COX-2 selectivity index (IC<sub>50</sub> COX-1/IC<sub>50</sub> COX-2).

<sup>c</sup> BHA, Salicylic acid.

the case that R<sub>4</sub> was N(Me)<sub>2</sub>, compound **27** with OH in C5 was the second-best one on COX-2 inhibition among all the compounds (IC<sub>50</sub> = 0.57 ± 0.13 μM), followed by compound **24** with H in C5 (compound **24**: IC<sub>50</sub> > 40 μM). Similarly, under the circumstances that R<sub>4</sub> was 2,3-di-Me-PhNH, compound **25** (IC<sub>50</sub> = 1.40 ± 0.13 μM) with OH in C5 also performed better than compound **22** (IC<sub>50</sub> = 2.31 ± 0.22 μM) with H in the same position. Besides, based on the parent compound **13**, the addition of methyl to C2' (compound **26**) or changing phenyl to methyl (compound **6**) led to the loss of activity (both IC<sub>50</sub> > 40 μM). The addition of substituents to C2' of phenyl rings also had some influence on COX-2 activity. Specifically, the addition of 2,3-dimethyl to phenyl rings in C2' had slightly increased (inhibitory effects on COX-2: compound **22** > compound **13**) or

decreased effects (inhibitory effects on COX-2: compound **16** > compound **25**), while the addition of 3-chloro-2-methyl to phenyl rings showed obviously decline of effects (inhibitory effects on COX-2: compound **20** < compound **14**, compound **19** < compound **8**, compound **1** < compound **13**).

Taking the data together, substituent of C5 was proved to be critical for the COX-2 inhibition potency. On the other hand, the selectivity study of COX demonstrated most of compounds (**2**, **3**, **8**, **9**, **14**, **18**) showed slight selectivity on COX-2, but only compounds **13** and **16** exhibited slight selectivity on COX-1. Given that both isoforms COX-1 and COX-2 played important roles in neuro-inflammation, inhibition on both COX-1 and COX-2 may be an advantage to take anti-neuroinflammatory effect [28].

### 2.3. Cell experiment

#### 2.3.1. Toxicity detection on C6 and BV2 cells

Both BV2 (mouse microglia cells) and C6 cells (rat astrocyte cells) as critical participants in neuroinflammation, are useful cell models to evaluate anti-neuroinflammation effects in vitro [52]. So LPS-induced C6 and BV2 cell experiments were conducted to screen potent anti-neuroinflammatory agents. Before cell assays, MTT assay was first performed to evaluate cytotoxicity of compounds on C6 and BV2 [53].

The results showed that cytotoxicity of compounds was divergent to a large extent, and was dramatically influenced by different substituents (Table 2). Among them, R<sub>4</sub> in C2' position had the largest impact on cytotoxicity. In C2' position, cytotoxicity was observed nearly in all compounds with phenyl substituted amine group (compounds **1**, **8**, **13**, **14**, **18**, **19**, **20**, **22**, **25**, **26**) but it was not observed in other compounds with hydroxyl, NMe<sub>2</sub> or NHMe groups. Moreover, the cytotoxicity order of compounds containing different substituents in C2' was phenyl substituted tertiary amine group > phenyl substituted secondary amine group. For instance, compound **26** with methyl(phenyl)amino substituent in C2' position had the strongest cytotoxicity (IC<sub>50</sub> = 7.98 ± 0.07 μM in BV2), while compound **13** with phenyl substituted secondary amine group had weaker cytotoxicity (IC<sub>50</sub> > 100 μM in BV2). In this regard, we speculated that due to high lipophilicity, compounds with phenyl substituted tertiary amine group on C2' may be easier to penetrate cell membrane than compounds with phenyl substituted secondary amine group. Besides, the cytotoxicity of compounds was also influenced by substituents in C5. When R<sub>4</sub> substituents in C2' position was a phenyl substituted amine, the toxicity order determined by C5 substituents was 5-Cl > 5-CH<sub>3</sub> > 5-OCH<sub>3</sub> > 5-OH and 5-H (compounds: **18** > **8** > **14** > **16** and **13**). Additionally, given that compounds **1**, **8**, **18**, **19**, **20**, **22**, **25**, **26** had obvious cell toxicity (IC<sub>50</sub> < 80 μM in either BV2 or C6), they were not considered for the following cell experiments.

#### 2.3.2. Inhibition of LPS-induced NO production in C6 and BV2 cell models

Nitric oxide (NO) as a main signal molecule produced in quantity by activated microglial and astrocytes, plays an important role in neuroinflammation. Although NO is normally regarded as neuroprotective factor in the brain, it can turn to be neurotoxic at specific circumstances. One important mechanism is that after pathological stimulation, NO produced by iNOS can react with superoxide to give peroxynitrite (ONOO<sup>·</sup>) which can stress or kill neurons and this process depends on the level of NO production [54–56]. Thus, inhibition of NO overproduction is considered as a

significant indicator of anti-neuroinflammation.

In this respect, the effects of compound on nitric oxide production in culture supernatant were evaluated by the Griess reagent [57]. As shown in Table 3, most of compounds displayed favorable inhibition on NO production in C6 and BV2 cells. Nevertheless, the inhibition of compounds on NO production was distinguishing, which was influenced by different substituents on C5, C2', C4' and C5'. The primary structure–activity relationships were demonstrated as follows:

- i) When R<sub>4</sub> in C2' was a hydroxyl, nature (H, F, Cl, OH, Me) and positions of substituents on phenyl rings were two decisive factors. In conclusion, in C4' position, the NO inhibitory potency order for these compounds was Me > H > F and OH (compounds: **3** > **23** > **12** and **7**). In detail, compound **3** with methyl in C4' had the best inhibition on BV2 cells (IC<sub>50</sub> = 4.94 ± 0.43 μM) and the third best inhibition on C6 cells (IC<sub>50</sub> = 7.48 ± 2.18 μM), in contrast, compound **7** with OH in C4' and compound **12** with F in C4' had no obvious effects in both cells (IC<sub>50</sub> > 40 μM). Interestingly, when methyl transferred to C5' position, like compound **11**, the activity markedly reduced (IC<sub>50</sub> > 40 μM). This great change demonstrated the importance of locations of substituents. Additionally, the change of substituents in C5' from methyl (compound **11**) to chlorine (compound **5**) did not influence the activity anyway. Similarly, substituents in C5, like OH and Me respectively in compounds **9** and **4**, had no promotion on effects. Better inhibitory effect was observed unexpectedly when the phenyl ring of salicylic acid moiety (compound **23**, IC<sub>50</sub> > 40 μM in C6 cells) was replaced by naphthyl ring (compound **2**, IC<sub>50</sub> = 13.24 ± 0.30 μM in C6 cells). This suggested enlarged conjugate plane contributed to down-regulation of NO production.
- ii) When R<sub>4</sub> in C2' was an amine, an important determinant affecting NO production was the substituent in R<sub>4</sub>. Specifically, compounds possessing phenyl-substituted secondary amine (compounds **13**, **14**, **16**) seemed more effective than those with methyl-substituted amine in C2' (compounds **6**, **24**, **27**). Besides, for compounds bearing phenyl-substituted secondary amine in C2', the substituents (H, OMe, OH) in C5 had a slight influence on potency (compounds **13**, **14**, **16** had close effects). But for compounds with dimethyl-substituted amine in C2', no substitution (compound **24**, IC<sub>50</sub> = 22.89 ± 1.82 μM in BV2 cells) in C5 performed a little better effect than that substituted with OH (compound **27**, IC<sub>50</sub> > 40 μM in BV2 cells) in the same position.

In view of the comprehensive evaluation of COX assay and NO assay, compounds **3**, **13** and **16** with outstanding effects were

**Table 2**  
Effects of compounds on viability of C6 and BV2 cells<sup>a</sup>.

Compd.	C6		BV2		Compd.	C6		BV2	
	Cytotoxicity IC <sub>50</sub> (μM) ± SD		Cytotoxicity IC <sub>50</sub> (μM) ± SD			Cytotoxicity IC <sub>50</sub> (μM) ± SD		Cytotoxicity IC <sub>50</sub> (μM) ± SD	
<b>1</b>	71.14 ± 12.80		54.60 ± 1.39		<b>14</b>	89.33 ± 3.10		>100	
<b>2</b>	>100		>100		<b>16</b>	>100		>100	
<b>3</b>	>100		>100		<b>18</b>	79.28 ± 0.91		62.36 ± 7.70	
<b>4</b>	>100		>100		<b>19</b>	66.11 ± 1.26		73.74 ± 0.05	
<b>5</b>	>100		>100		<b>20</b>	62.40 ± 0.06		>100	
<b>6</b>	>100		>100		<b>22</b>	95.23 ± 0.34		55.13 ± 0.80	
<b>7</b>	>100		>100		<b>23</b>	>100		>100	
<b>8</b>	87.86 ± 0.06		64.64 ± 8.76		<b>24</b>	>100		>100	
<b>9</b>	>100		>100		<b>25</b>	80.51 ± 4.07		56.42 ± 8.46	
<b>11</b>	>100		>100		<b>26</b>	28.54 ± 1.45		7.98 ± 0.07	
<b>12</b>	>100		>100		<b>27</b>	>100		>100	
<b>13</b>	115.24 ± 0.45		>100						

<sup>a</sup> C6 and BV2 cell lines were exposed to different compounds at 0, 6.25, 12.5, 25, 50, and 100 μM for 24 h. Then cell viability was detected by MTT method. IC<sub>50</sub> values were shown as the mean ± SD of triplicate in three independent experiments.

**Table 3**  
Effects of compounds on NO production in LPS-stimulated C6 and BV2 cells.<sup>a</sup>

Compd.	C6 cell IC <sub>50</sub> (μM)	BV2 cell IC <sub>50</sub> (μM)	Compd.	C6 cell IC <sub>50</sub> (μM)	BV2 cell IC <sub>50</sub> (μM)
<b>2</b>	13.24 ± 0.30	58.97 ± 5.76	<b>12</b>	>40	>40
<b>3</b>	7.48 ± 2.18	4.94 ± 0.43	<b>13</b>	15.30 ± 0.55	25.87 ± 5.74
<b>4</b>	>40	>40	<b>14</b>	7.61 ± 1.58	19.88 ± 0.99
<b>5</b>	>40	>40	<b>16</b>	6.73 ± 0.17	37.18 ± 1.73
<b>6</b>	>40	>40	<b>23</b>	>40	26.40 ± 2.57
<b>7</b>	>40	>40	<b>24</b>	>40	22.89 ± 1.82
<b>9</b>	>40	>40	<b>27</b>	>40	>40
<b>11</b>	>40	>40			

<sup>a</sup> The astrocyte (C6) and microglia cells (BV2) were exposed to the compounds for 24 h in the presence of LPS (10 μg/mL) and LPS (1 μg/mL) respectively. IC<sub>50</sub> (μM), the concentrations of compounds producing 50% inhibition of NO production in vitro compared to control. (IC<sub>50</sub>) values were determined by a dose-response inhibition curve with GraphPad PRISM. The data were shown as mean ± SD. All assays were performed in triplicate with data pooled from at least three independent experiments.

selected for further tests to explore their effects on inflammatory cytokine production of two glial cells.

### 2.3.3. Effects of compounds on LPS-induced TNF-α, PGE<sub>2</sub> and IL-10 production in C6 and BV2 cells

Neuroinflammation is a characteristic of many neurodegenerative diseases in which procedure microglia and astrocytes have been implicated to play both causative and exacerbating roles [58,59]. In fact, microglia and astrocyte keep mutual cooperation but play various roles by releasing a series of inflammatory mediators such as arachidonic acid metabolites (PGE<sub>2</sub>) and cytokines including tumor necrosis factor-alpha (TNF-α), interleukin-10 (IL-10) in responses to pathological stimulus [28]. In this regard, evaluation of cytokines or arachidonic acid metabolites of both glial cells was performed to assess anti-neuroinflammation of synthesized compounds in vitro.

As illustrated in Fig. 1A, TNF-α as a principal pro-inflammatory mediator released by activated microglia was measured by ELISA method. Its production markedly increased compared to control group after LPS treatment (1 μg/mL). Compounds **3** and **13** specifically inhibited LPS-induced TNF-α production in a concentration-dependent manner. Among the three tested hybrids, compound **13** was the most potential to inhibit secretion of TNF-α, followed by compounds **3** and **16**. Besides, as shown in Fig. 1B, TNF-α released by activated astrocyte was also measured by using the same way. Its production was ascended compared to control group after being treated by a higher concentration of LPS (10 μg/mL). The difference in LPS concentration capable of activating glial cells indicated that microglia as the first defense of immunity in brain, may be easier to be activated by LPS compared to astrocyte [60]. Similarly, the inhibitory effects of compounds **3**, **13** and **16** were also found in a dose-dependent manner in LPS-induced astrocyte cell model. Being identical with the results of LPS-induced microglia cell model, compound **13** was the most potential to inhibit secretion of TNF-α in astrocyte cells, followed by compounds **3** and **16** in astrocyte cells.

On the other hand, PGE<sub>2</sub> is also a well-known inflammatory mediator derived from arachidonic acid via the action of cyclooxygenases. It is produced in large quantities by activated microglia which expresses the mPGES [28]. As shown in Fig. 1C, production of PGE<sub>2</sub> by activated microglia distinctly increased after LPS treatment (1 μg/mL) compared to the control group. Compounds **3** and **16** particularly inhibited LPS-induced production of PGE<sub>2</sub> in a concentration-dependent manner. Unlike the results of TNF-α in LPS-induced microglia cell model, compound **3** was the most potential, followed by compounds **16** and **13**. Considering that over-production of PGE<sub>2</sub> is associated with up-regulation of COX-2 [61], so we postulated that these tested compounds may take effect by down-regulating COX-2 or inhibiting COX-2. The detailed discussion on it was shown in western blotting assay (Fig. 2).

In the neuroinflammatory procedure, the signals responsible for turning on and off microglia have long been put in a dominant position because these signals could contribute to immune surveillance and homeostasis in the CNS. On the other hand, Interleukin-10 (IL-10) has been proved to implicate in limiting microglia activation and CNS inflammation [62]. In this respect, we chose IL-10 production as one of the evaluation criterias for anti-neuroinflammation. As shown in Fig. 1D, production of anti-inflammatory mediator IL-10 released by activated microglia dramatically increased compared to control group after LPS treatment (1 μg/mL). This phenomenon suggested that there was also an acute response to LPS via the secretion of the anti-inflammatory cytokine IL-10 in enriched microglia [63]. Compounds **3** and **16** significantly up-regulated the production of IL-10 in 40 μM, but compound **13** showed no obvious effects in this regard (IC<sub>50</sub> > 40 μM) compared to LPS group. Combining this result with the above results on TNF-α and PGE<sub>2</sub> production, we concluded the anti-neuroinflammation of compounds **3** and **16** in 40 μM depended partially on the balance between pro-inflammation and anti-inflammation via regulation of immunosuppressive and anti-inflammatory mediators.

In a word, overall data on cytokines (TNF-α, IL-10), NO, arachidonic acid metabolites (PGE<sub>2</sub>) confirmed the effects of compounds **3**, **13** and **16** on two crucial participants (microglia and astrocytes) in neuroinflammation, although the degree of influence varies with the compounds. Subsequently, the possible reasons to explain this disparity in NO and PGE<sub>2</sub> regulation were discussed by western blotting assay.

### 2.3.4. Effects of compounds on LPS-induced iNOS and COX-2 production in C6 and BV2 cells

To explain the reasons for the discrepant inhibition effects of compounds on nitric oxide (NO) and PGE<sub>2</sub> production, the western blotting assay was performed in BV2 and C6 cells.

Given that NO as a free radical, can be produced by inducible NO synthase (iNOS) isoform, we preliminarily tested the expressions of iNOS in microglia and astrocyte. As shown in Fig. 2A, unstimulated microglia cells expressed extremely low levels of iNOS protein which is consistent with the character of a non-activation state of microglia. After being stimulated by LPS for 24 h (1 μg/mL), the expression of iNOS in BV2 cells soared. However, iNOS expression drastically decreased by compounds **3** and **13** treatment compared to LPS group. Combining the results of NO assay and iNOS assay, compound **3** performed the best (IC<sub>50</sub> = 4.94 ± 0.43 μM for NO inhibition, 100% reduction of iNOS at 40 μM), then compound **13** came second (IC<sub>50</sub> = 25.87 ± 5.74 μM for NO inhibition, 66% reduction of iNOS at 40 μM) and followed by **16** (IC<sub>50</sub> = 37.18 ± 1.73 μM for NO inhibition, no obvious reduction of iNOS at 40 μM) in both assays, indicating the consistency of two assays. On the other hand, the expression of iNOS was also

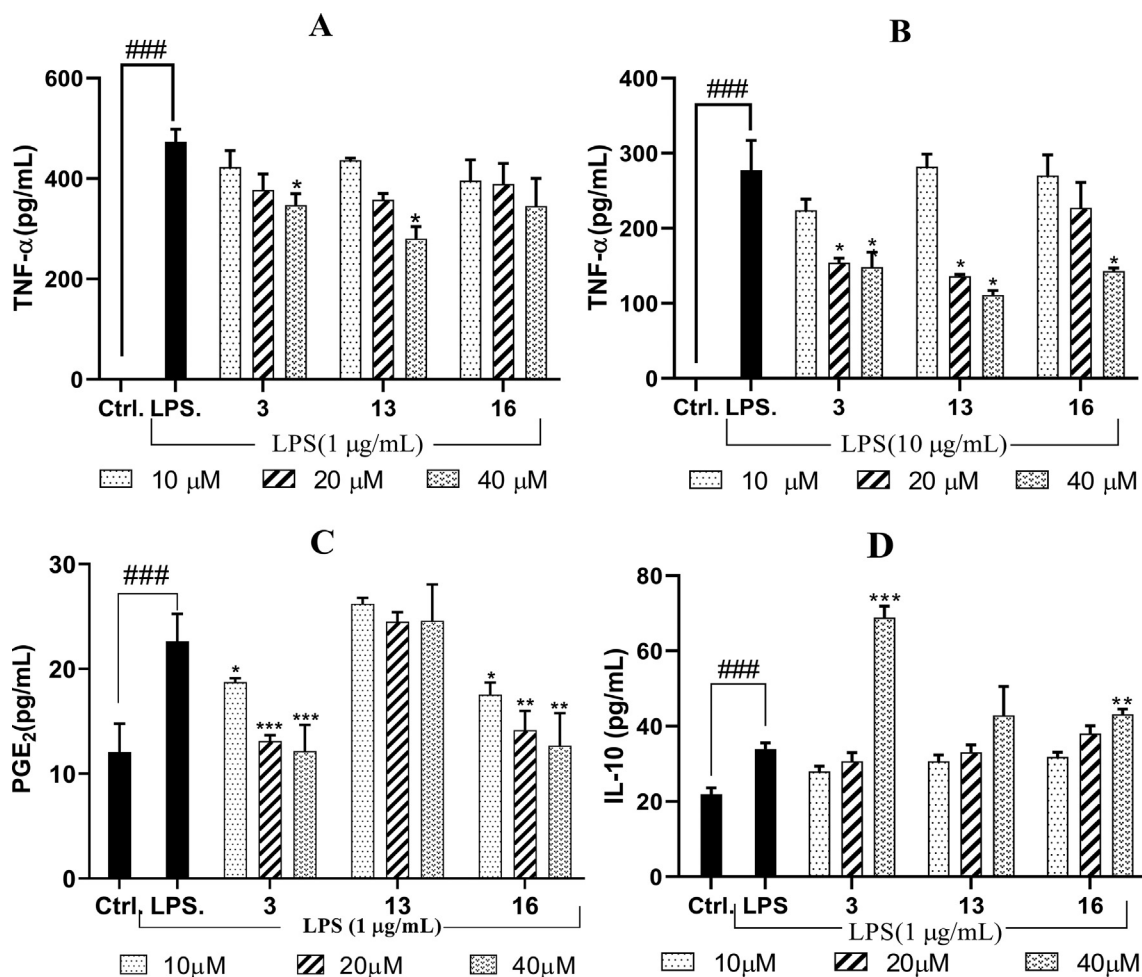


**Fig. 1.** Effects of compounds on TNF- $\alpha$  (Fig. 1, A), PGE<sub>2</sub> (Fig. 1, C), IL-10 (Fig. 1, D) in LPS-stimulated BV2 cells and effects on TNF- $\alpha$  in C6 cells (Fig. 1, B). BV2 cells were exposed to compounds 3, 13, 16 at concentrations of 10, 20, and 40  $\mu$ M for 24 h in the presence of LPS (1  $\mu$ g/mL). C6 cells were exposed to compounds 3, 13, 16 at concentrations of 10, 20, and 40  $\mu$ M for 24 h in the presence of LPS (10  $\mu$ g/mL). Each error bar represents the mean  $\pm$  SD of three independent experiments. ###,  $p < 0.001$ , when compared to control cells. \*,  $p < 0.05$ , \*\*,  $p < 0.01$ , \*\*\*,  $p < 0.001$ , when compared to the LPS-treated cells. All data are the mean  $\pm$  SD of at least three independent experiments. Ctrl. means the control group. LPS means the LPS-treated group.

markedly up-regulated when astrocytes response to stimuli [64]. As shown in Fig. 2B, the expression of iNOS in astrocytes increased significantly compared to control after LPS treatment. When treated by compounds 3 and 16, an obvious decrease was also found in LPS-induced astrocytes. Similarly, compound 16 ( $IC_{50} = 6.73 \pm 0.17 \mu$ M for NO inhibition in C6 cells, 95% reduction of iNOS at 40  $\mu$ M) performed better than compound 3 ( $IC_{50} = 7.48 \pm 2.18 \mu$ M for NO inhibition in C6 cells, 29% reduction of iNOS at 40  $\mu$ M) in both assays.

Besides, the decrease of PGE<sub>2</sub> production was associated with down-regulation of COX-2 or inhibition effects on COX-2 [28,65,66]. As shown in Fig. 2A, the expression of COX-2 protein significantly increased in BV2 cells induced by LPS (1  $\mu$ g/mL) stimulation, demonstrating that COX-2 has emerged as one of the major players in brain inflammation, and increased COX-2 expression was believed to contribute to neurodegeneration [67]. Besides, inhibitory effect on the expression of COX-2 can be observed by compounds 13 and 16. Different from those compounds, compound 3 showed no obvious effects on COX-2 expression. Referring to the results of three assays (COX inhibition, COX-2 expression and PGE<sub>2</sub> estimation), we speculated that compound 3 was more likely to reduce the production of PGE<sub>2</sub> by inhibiting COX-2, because compound 3 ( $IC_{50} = 4.16 \pm 0.43 \mu$ M for COX-2) had outstanding

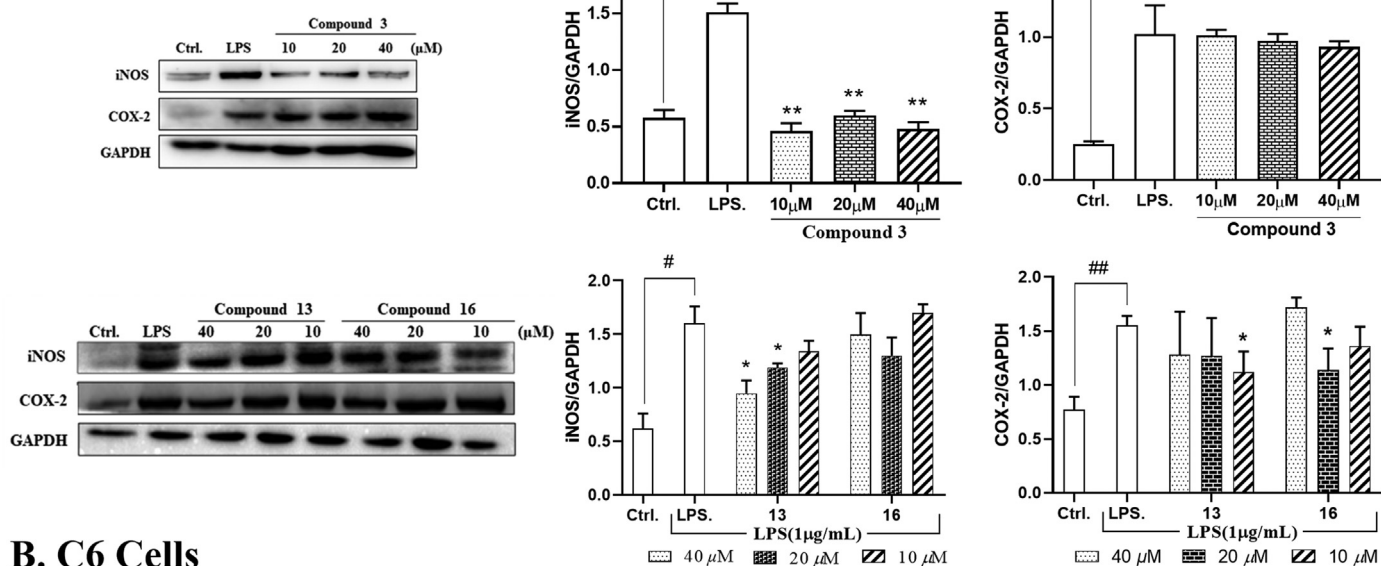
inhibitory effects on COX-2 but could not down-regulate COX-2 expression ( $IC_{50} > 40 \mu$ M). Additionally, compounds 3, 13 and 16 with favorable anti-neuroinflammation potency are worth further investigations.

### 2.3.5. Inhibition effects on LPS-induced ROS production in BV2 cells

Microglia as one of the first defense lines protecting CNS against injury, can be quickly activated in response to CNS injuries or immunologic stimuli. However, its sustained activation is apt to result in overproduction of various proinflammatory and neurotoxic substances. In addition to nitric oxide (NO), cytokines, arachidonic acid (AA) and its metabolites, excess intracellular ROS produced in this process can also induce mitochondria oxidative damage and eventually cause cell death [68,69]. Worse still, if extracellular ROS continuously released by microglia, neuronal injuries ensue, which is related to neurodegenerative diseases [70,71]. Therefore, by lowering the levels of highly versatile ROS, neuroinflammatory cascades are expected to be hindered and the aim of neuroprotective would be achieved.

The results showed that after LPS treatment (Fig. 3, green lines), levels of ROS significantly increased compared to the control group (Fig. 3, red lines), indicating that inflammation cascade responses occurred immediately (determined at 6 h). Afterwards, a decrease

## A. BV2 Cells



## B. C6 Cells

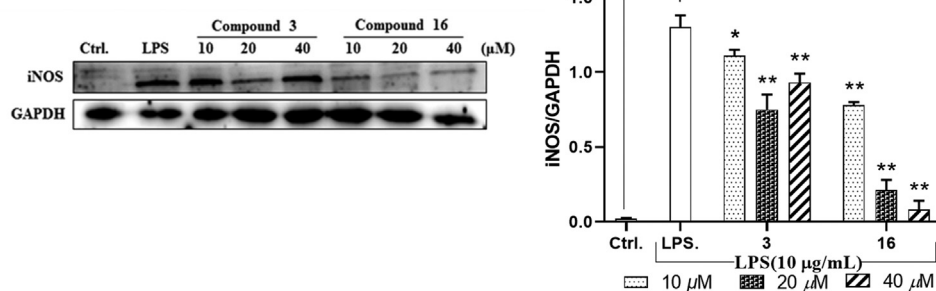


**Fig. 2.** Effects of compounds on protein expressions of iNOS, COX-2 in LPS-induced BV2 cell lines (A) and effects of compounds on protein expressions of iNOS in LPS-induced C6 cell lines (B). BV2 cell lines were exposed to the indicated compounds at concentrations of 10, 20 and 40  $\mu$ M for 24 h in the presence of LPS (1  $\mu$ g/mL). C6 cell lines were exposed to the indicated compounds at concentrations of 10, 20 and 40  $\mu$ M for 24 h in the presence of LPS (10  $\mu$ g/mL). The expression of iNOS and COX-2 was assayed and calculated by image J. Each error bar represents the mean  $\pm$  SD of three independent experiments. #,  $p < 0.05$  versus the control group; ##,  $p < 0.01$  versus the control group; ###,  $p < 0.001$  versus the control group. \*,  $p < 0.05$ , \*\*,  $p < 0.01$  when compared to the LPS-treated cells. All data are the mean  $\pm$  SD of at least three independent experiments.

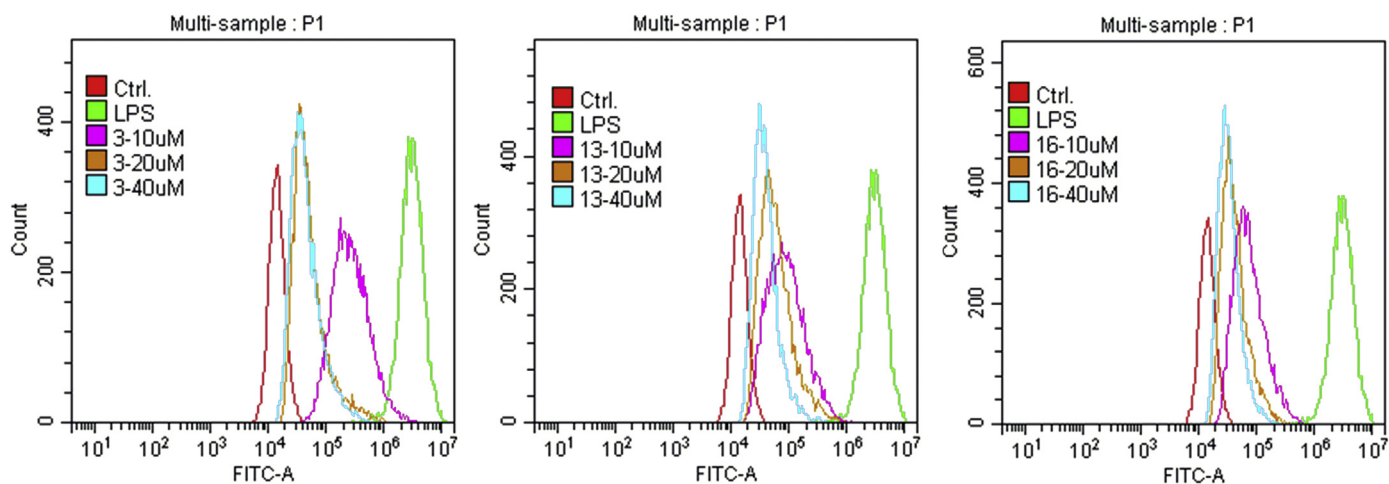


**Fig. 3.** Effects of compounds 3, 13 and 16 on ROS generation in LPS-stimulated BV2 Cells. Compounds 3, 13 and 16 clearly attenuated LPS-induced production of reactive oxygen species (ROS). The data were detected at 6 h after LPS stimulation (1  $\mu$ g/mL). ROS production was determined by a fluorescence probe DCFH-DA.

of ROS production was observed by compounds **3**, **13** and **16** treatment, which suggested that compounds **3**, **13** and **16** significantly reduced inflammation response in LPS-induced BV2 cells. To discuss the reason of ROS reduction, the following DPPH assay was conducted to evaluate radical scavenging potency of these compounds.

#### 2.3.6. Evaluation of radical scavenging potency by DPPH assay

The radical scavenging capacity was evaluated using 2,2-diphenyl-1-picrylhydrazyl (DPPH) method [72]. DPPH being composed of unstable free radical traps any radicals produced by the tested compounds and brings about a visible color change ranging from violet to pale yellow to colorless. The degree of the changes in comparison to the control was calculated as radical scavenging capacity. As shown in Table 4, the results showed that 5-OH substituted compound **16** was more potent than non-5-OH-substituted compound **13**, and this may be due to the free radical quenching of 5-OH group. Moreover, compounds **3** and **16** exhibited low EC<sub>50</sub> indicating that the phenol hydroxyl is a kind of good free radical quenchers. The results of compounds **3** and **16** were consistent with that of ROS production. These data suggested that compounds substituted with phenol hydroxyl group were found to be the potential radical scavenger which may have to do with decreasing the production of reactive oxygen species (ROS). However, compound **13** was inactive in DPPH assay but showed good effect in LPS-induced ROS production in BV2 cells. The possible reason for this observation was that compound **13** may take effect by influencing antioxidant related signaling pathway.

In sum, compounds **3** and **16** had multifunctional anti-neuroinflammation activities in vitro, including COX inhibitory effects, cytokines inhibitory effects as well as radical scavenging capacity. The following immunofluorescence staining assay evaluated the effects of tested compounds on glial activation to confirm their potency of anti-neuroinflammation.

#### 2.3.7. Inhibitory effects on activation of LPS-induced astrocytes and microglial cells

Neuroinflammation is closely related to the activation of microglia and astrocytes [73,74]. The increased expressions of glial fibrillary acidic protein (GFAP) and ionized calcium-binding adapter molecule 1 (Iba-1), which was respectively considered as the inflammatory response of rat astrocytes (C6) and microglia (BV2) induced by LPS, serve as the pathological hallmarks of various neuroinflammation related diseases including Multiple Sclerosis and Alzheimer's disease. Thus, anti-neuroinflammatory effects of compounds can be evaluated by immunofluorescence labelling of GFAP and Iba-1.

As seen in Fig. 4A, the expression of GFAP in C6 cell increased significantly after being stimulated by LPS (10 µg/mL). But after compounds **3**, **13** and **16** treatment (20 µM), the expressions of GFAP significantly reduced by observing under the same laser intensity, indicating that selected compounds **3**, **13** and **16** could inhibit the activation of rat astrocytes. Similarly, the above tendency was also observed in LPS-induced BV2 cells model. As shown in Fig. 4B, the expression of Iba-1 in BV2 cell increased by LPS

treatment (1 µg/mL). However, after compounds **3**, **13** and **16** treatment (20 µM), all the expression of Iba-1 declined noticeably. Among them, compounds **3** and **13** showed better potency on two glial cells. The above results reaffirmed the inhibitory effects of compounds **3**, **13** and **16** on activation of astrocytes and microglial cells.

#### 2.4. LPS-induced neuroinflammation in mice

In view of the outstanding effects on cell models and inhibition on COX-2 (IC<sub>50</sub> = 4.16 ± 0.43 µM for compound **3**, IC<sub>50</sub> = 0.50 ± 0.10 µM for compound **16**), compounds **3** and **16** were chosen for in vivo study. LPS was used to induce neuroinflammation in mice, for which could trigger a series of CNS inflammatory reactions and consequently lead to neuronal damage [75,76].

Mice were injected intraperitoneally by LPS for six days then sacrificed for pharmacodynamic evaluation. Considering that the activation of astrocytes and microglia are regarded as a key event in the neuroinflammatory process, we investigated inhibitory effects of compounds **3** and **16** on glial cells activation. Fig. 5 showed that a higher level of Iba-1 (a marker of activated microglia) and GFAP (a marker of activated astrocytes) in the hippocampi of mice treated with LPS were observed compared to the sham group, confirming the success of modelling. When treated by compounds **16** or **3** (50 mg/kg, i.p., twice a day), levels of GFAP for both compounds and Iba-1 for compound **3** in the mouse hippocampus significantly reduced compared to LPS treated group (Fig. 5, A-D). In addition, Iba-1 and GFAP expression in hippocampus regions were also evaluated by western blotting method (Fig. 5E). The western blotting results were consistent with that of immunofluorescence staining. Unexpectedly, melatonin did not display the expected effect of attenuating glial cell activation (p > 0.05), which was inconsistent with the previous reports [9,13]. The possible reason could be different methods of administration (intraperitoneal injection in our work and oral administration in reported works) and high dosage of melatonin (50 mg/kg, twice a day) [77–80]. We observed that mice were lethargic and 40% of melatonin group died within six days, while in compounds **3** and **16** group, no abnormal behaviors or death happened. Therefore, we concluded that compounds **3** and **16** are safer and more effective than melatonin under the specific administration. In addition, salicylic acid showed the capability of inhibiting microglial cell activation, but the effect was weaker than that of compound **3**. The above results show that the combination of salicylic acid and melatonin not only can enhance the anti-neuroinflammatory effect but also ensure safety (more toxicity data were shown in 2.5).

To determine the extent of neuronal damage after LPS treatment, Nissl staining was performed on hippocampal tissue slices of mice. In accordance with the above results, Nissl staining results revealed that LPS treatment increased damage of neuron, as shown by damaged, fragmented or shrunken neuronal cells (Fig. 6, indicated by the black mark). Administration of compounds **3** or **16** attenuated damage of neurons, as shown by the more integral neuron than the LPS treated group. In addition, there was significant apoptosis in CA1 by salicylic acid treatment. Additionally, the melatonin group also showed significant neuronal apoptosis (marked by black arrows), indicating that high dosage of melatonin by intraperitoneal injection had no obvious neuroprotective effect.

Overall, these results demonstrated that N-salicyloyl tryptamine derivatives exerted inhibition on neuroinflammation, had promising therapeutic potency, and should be new drug candidates for neuroinflammation treatment, which is a widely proved pathomechanism in Alzheimer's or other CNS diseases.

**Table 4**  
In vitro antioxidant activity by DPPH method.

Compd.	EC <sub>50</sub> (µM) <sup>a</sup>	Compd.	EC <sub>50</sub> (µM) <sup>a</sup>
<b>3</b>	25.18 ± 2.99	<b>Melatonin</b>	>40
<b>13</b>	>100	<b>5-HT<sup>b</sup></b>	0.63
<b>16</b>	3.82 ± 1.10		

<sup>a</sup> EC<sub>50</sub>, concentration which possesses 50% radical scavenging ability.

<sup>b</sup> 5-Hydroxytryptamine.

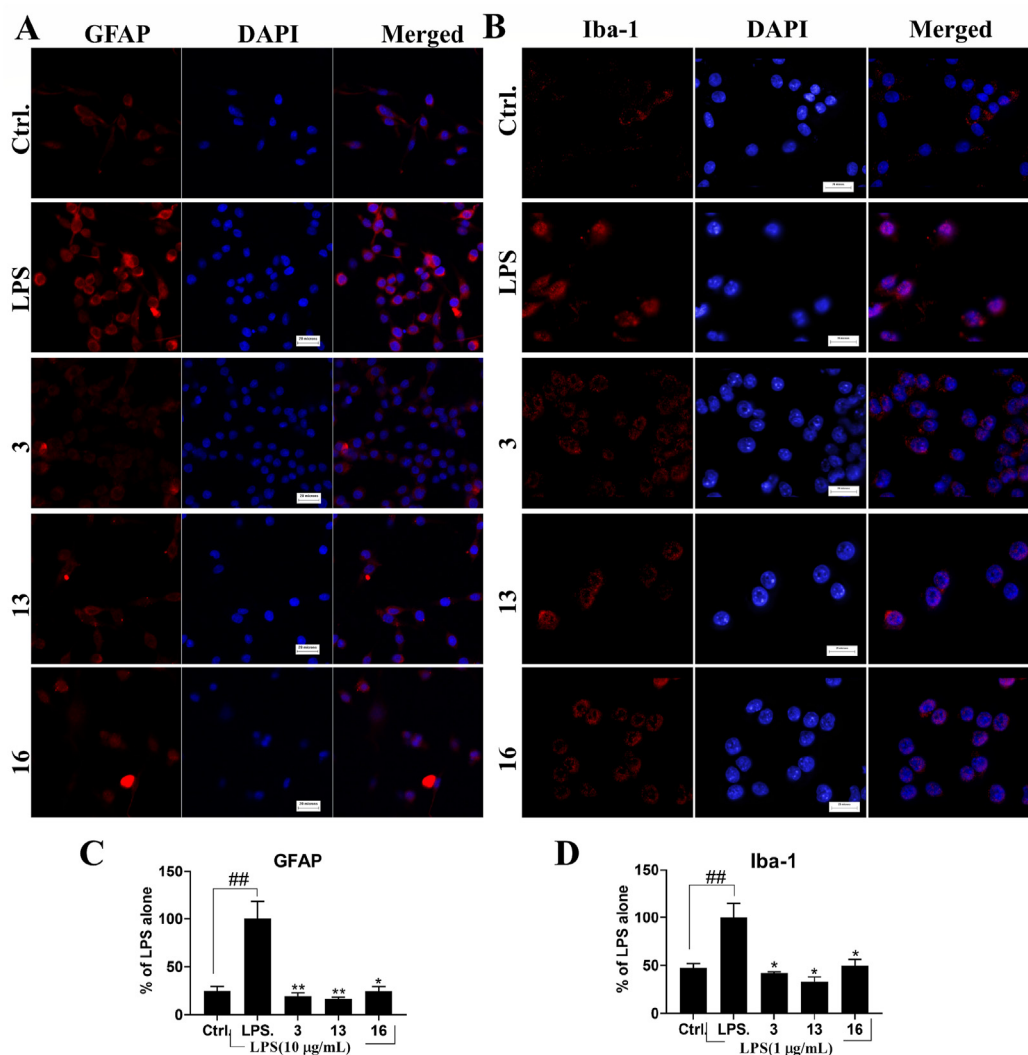


**Fig. 4.** Effects of compounds on GFAP and Iba-1 expression in the LPS-induced astrocytes (C6, treated with 10  $\mu\text{g/mL}$  of LPS) and microglia (BV2, treated with 1  $\mu\text{g/mL}$  of LPS). **A.** Representative fluorescence microscopy images of GFAP immunostaining (Magnification  $\times 20$ ). **B.** Representative fluorescence microscopy images of Iba-1 immunostaining (Magnification  $\times 40$ ). **C.** Histograms show relative changes of GFAP expressed as mean  $\pm$  SD of the three independent experiments ( $n = 3$ ). Ctrl. = Control, LPS = Lipopolysaccharide (10  $\mu\text{g/mL}$ ); **3**, **13**, **16** = treatments by compounds **3**, **13**, **16** (20  $\mu\text{M}$ ) along with LPS (10  $\mu\text{g/mL}$ ). **D.** Histograms show relative changes of Iba-1 expressed as mean  $\pm$  SD of the three independent experiments ( $n = 3$ ). All the data were analyzed using Image Pro Plus and expressed as a percent of LPS group values (fluorescence intensity). (#) Significant difference ( $##p < 0.01$ ,  $###p < 0.001$ ) vs. control and (\*) significant difference ( $*p < 0.05$  and  $**p < 0.01$ ) vs. LPS.

### 2.5. Acute toxicity study for compounds **3** and **16** in mice

Acute toxicity studies with compounds **3** and **16** were performed on ten mice according to OECD guidelines [81]. All treatments were given orally in a single dose of 1000 mg/kg, and the animals showed no any signs of behavioral alterations upon treatment with compounds **3** and **16**. At the end of 14 days, the animals were sacrificed for gross examination of heart, liver, kidney or stomach. Gross examination and histological examination did not reveal any significant alterations in the heart, liver, kidney or stomach when compared to vehicle treated control (Fig. 7). The results suggested that the oral  $\text{LD}_{50}$  of compounds **3** and **16** in mice is higher than 1000 mg/kg.

### 2.6. Pharmacokinetic study

The pharmacokinetic properties of compounds **3** and **16** were examined in male SD rats by intraperitoneal injection. As shown in Table 5, compounds **3** and **16** displayed different pharmacokinetic

characters. After intraperitoneal injection, compounds **3** and **16** were both easily absorbed into plasma, with  $T_{\text{max}}$  values of  $0.19 \pm 0.10$  h and  $0.92 \pm 0.14$  h respectively. However, compound **3** showed approximately 3-fold lower  $C_{\text{max}}$  value ( $C_{\text{max}} = 2.10 \pm 0.22$   $\mu\text{g/mL}$ ) than that of compound **16** ( $C_{\text{max}} = 6.08 \pm 2.39$   $\mu\text{g/mL}$ ). A possible explanation for these results was that compound **16** was more easily absorbed than compound **3** owing to the higher LogP value of compound **16**. Besides, compound **16** had a short half-life ( $t_{1/2} = 2.72 \pm 0.75$  h) which may attribute to easy elimination of hydroxyl in C5 position. Compared to melatonin featured a short plasma half-life ( $0.54 \pm 0.22$  h), compounds **3** and **16** had prolonged plasma half-life ( $13.95 \pm 4.66$  h and  $2.72 \pm 0.75$  h respectively), these findings support the combination strategy promotes the pharmacokinetic profiles.

### 3. Conclusion

In summary, a new series of N-salicyloyl tryptamine derivatives were synthesized based on the combination of melatonin and

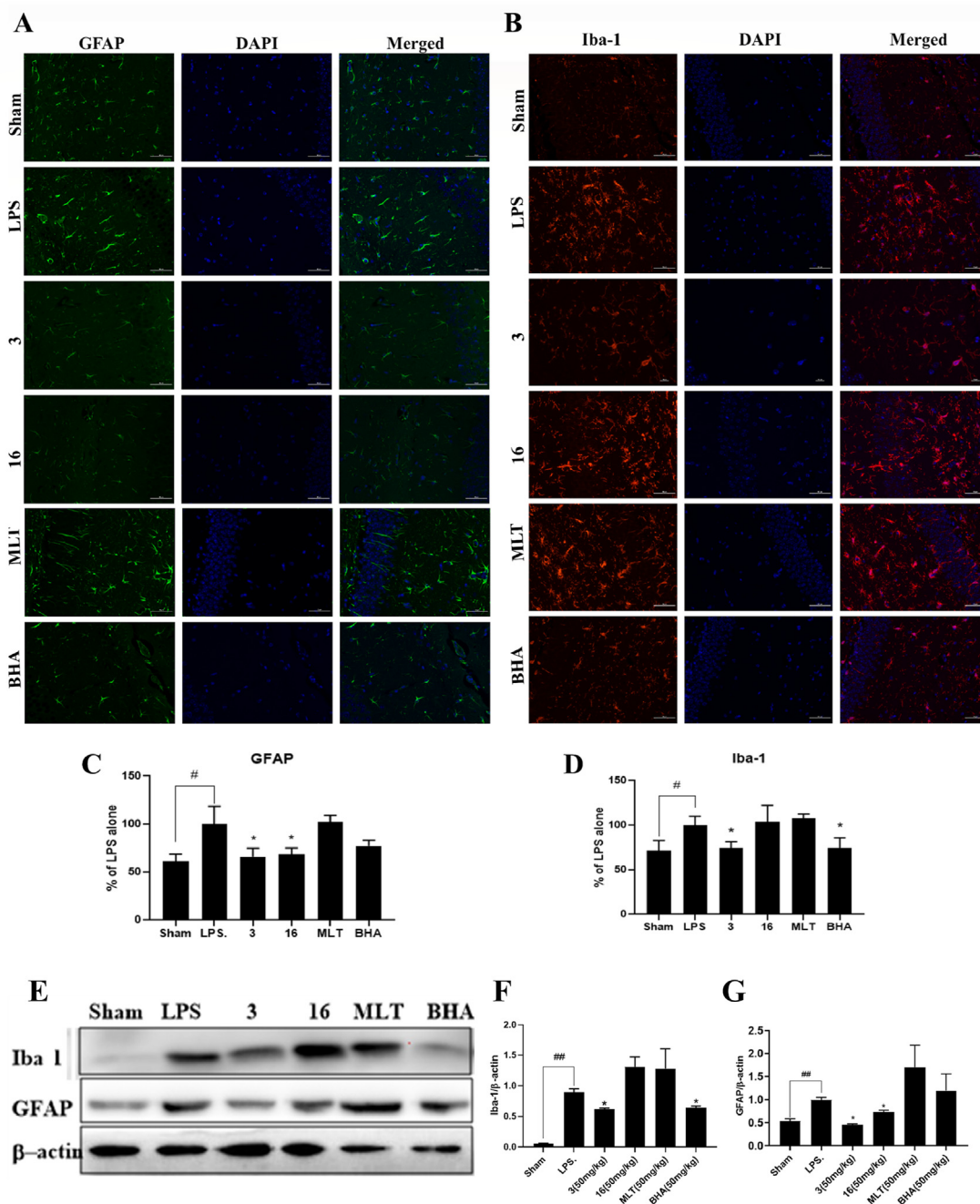


**Fig. 5.** Effects of compounds **3**, **16**, **MLT**, **BHA** on expressions of GFAP and Iba-1 in LPS-induced hippocampal impairment of male mice. Sham. = Sham-operated mice were injected with 3  $\mu$ L of saline. LPS = Lipopolysaccharide (3  $\mu$ L, 10 mg/mL). **3**, **16**, **MLT**, **BHA** = respectively treated by compounds **3**, **16**, **MLT**, **BHA** (50 mg/kg, i.p. twice daily for six consecutive days) after LPS injection (3  $\mu$ L, 10 mg/mL). **A.** Representative fluorescence microscopy images of GFAP immunostaining (Magnification  $\times$  40, scale bar = 50  $\mu$ m). **B.** Representative fluorescence microscopy images of Iba-1 immunostaining (Magnification  $\times$  40, scale bar = 50  $\mu$ m). **C.** Histograms showed relative fluorescence intensity of GFAP levels referring to LPS group values, and expressed as mean  $\pm$  SD (groups (n = 6) except for melatonin group (n = 3)). **D.** Histograms showed relative fluorescence intensity of Iba-1 levels referring to LPS group values, and expressed as mean  $\pm$  SD (groups (n = 6) except for melatonin group (n = 3)). All the immunofluorescence data were analyzed using Image pro plus software. **E.** Western blot image of Iba-1 and GFAP. **F.** Qualification of GFAP expression (groups (n = 4) except for melatonin group (n = 3)). **G.** Qualification of Iba-1 expression (groups (n = 4) except for melatonin group (n = 3)). (#) Significant difference ( $\#p < 0.05$ ,  $\#\#p < 0.01$ ) vs. control and (\*) significant difference ( $*p < 0.05$  and  $**p < 0.01$ ) vs. LPS.

salicylic acid for the treatment of neuroinflammation with multifunctional profiles. Several biological assays in vitro and in vivo were conducted and proved N-salicyloyl tryptamine derivatives as multifunctional agents to treat neuroinflammation. In COX inhibitor screening assay, synthesized compounds exhibited diversely inhibitory effects with  $IC_{50}$  values ranging from 0.50 to more than 40  $\mu$ M. Among them, 15 compounds showed extremely better inhibition on COX-2 than salicylic acid. Additionally, most of

compounds (**2**, **3**, **8**, **9**, **14**, **18**) showed slight selectivity on COX-2. The detailed structure–activity relationships on COX-2 inhibition indicated that the substitution of C5 was crucial for the COX-2 inhibition potency. To evaluate the anti-neuroinflammation in vitro, LPS-induced BV2 and C6 cell models were used. The cytotoxicity assay showed compounds with phenyl substituted amine group in C2' had obvious cytotoxicity on C6 or BV2. For inhibition on NO production of C6 and BV2, most of compounds displayed favorable

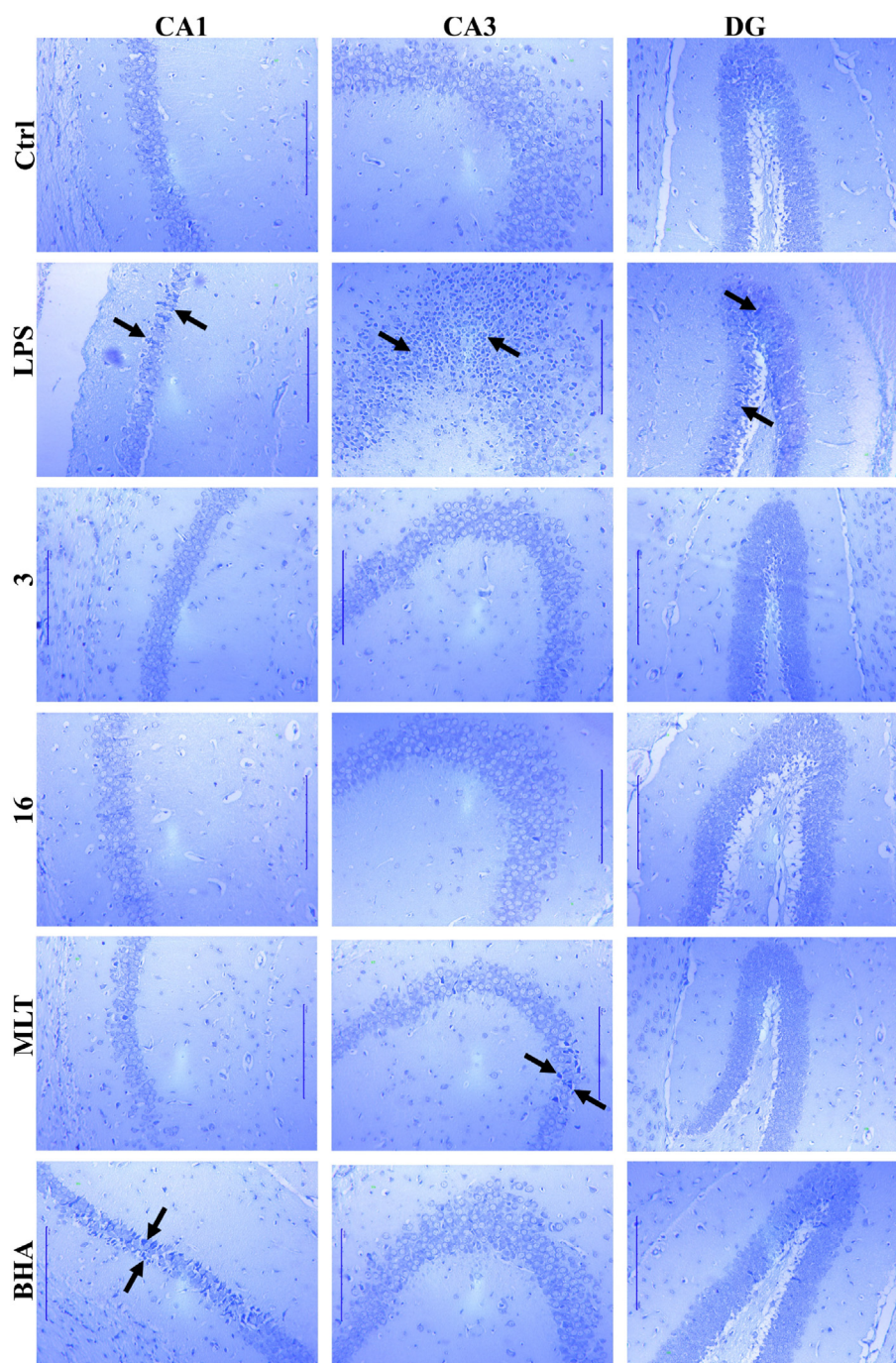


**Fig. 6.** Effects of selected compounds on LPS-induced neuron death in the hippocampus region. The sections of the hippocampus region were stained by Nissl (magnification  $40\times$ , scale bar =  $100\ \mu\text{m}$ ). The black arrow marked the position where neuronal cells disappeared or were sparse with pyknotic cell nucleus and even were induced to apoptosis. (For interpretation of the references to color in this figure legend, the reader is referred to the Web version of this article.)

effects. Comprehensively analyzing the results of NO production and COX inhibitor screening assay, compounds **3**, **13** and **16** were chosen for further studies. From results of cytokines (TNF- $\alpha$ , IL-10), PGE<sub>2</sub>, all compounds **3**, **13** and **16** took effects on both glial cells although their effects were in great difference. Western blotting assay measuring expressions of iNOS and COX-2 showed that compounds **3** and **13** significantly down-regulated the expressions of iNOS in BV2 and C6 cells, furthermore, compounds **13** and **16** significantly down-regulated the expressions of COX-2 in BV2 cells. In ROS release assay, compounds **3**, **13** and **16** significantly

attenuated LPS-induced production of reactive oxygen species (ROS), but only compounds **3** and **16** had radical scavenging capacity in DPPH assay. In this respect, compound **13** may take effect by influencing antioxidant related signaling pathway. The immunofluorescence results reconfirmed the inhibitory effects of compounds **3**, **13** and **16** on activation of astrocytes and microglial cells. In LPS-induced neuroinflammation model in mice, administration of compounds **3** and **16** by intraperitoneal injection at the dose of 50 mg/kg suppressed the activation of astrocyte cells, but only compound **3** attenuated the activation of microglia cells. Nissl

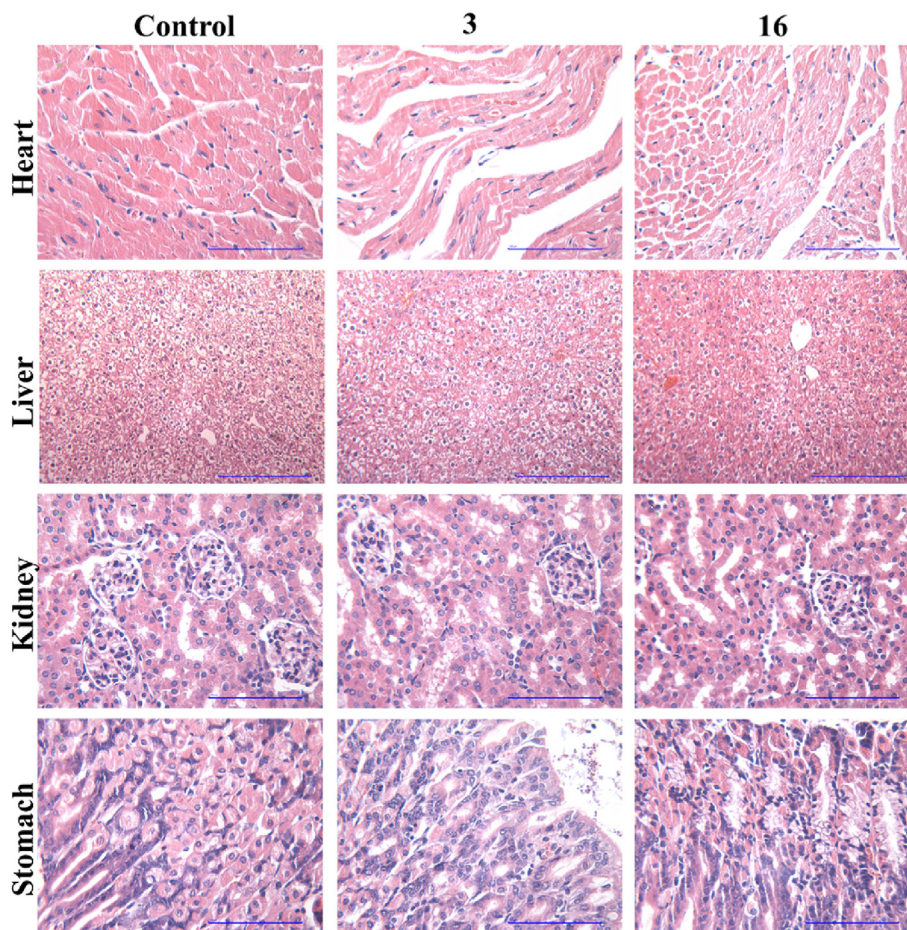


**Fig. 7.** Histologic specimens of mice tissues (heart, liver, kidney and stomach) in vehicle treated control, compound **3** treated group (1000 mg/kg) and compound **16** treated group (1000 mg/kg) which were stained with hematoxylin and eosin ( $n = 10$ , five male and five female mice). Images of histology heart, liver and kidney zoomed in 40 times.

**Table 5**  
Pharmacokinetic profiles for compounds **3** and **16** in SD rats.

Parameter	Compound 3	Compound 16	Melatonin
$t_{1/2}$ (h)	$13.95 \pm 4.66$	$2.72 \pm 0.75$	$0.54 \pm 0.22$
$T_{max}$ (h)	$0.19 \pm 0.10$	$0.92 \pm 0.14$	$0.19 \pm 0.18$
$C_{max}$ ( $\mu\text{g/mL}$ )	$2.10 \pm 0.22$	$6.08 \pm 2.39$	$1.15 \pm 0.04$
$AUC_{0-t}$ ( $\mu\text{g/mL} \times \text{h}$ )	$14.39 \pm 1.67$	$12.46 \pm 3.55$	$0.98 \pm 0.32$
MLogP	2.25	2.86	0.97

<sup>a</sup>Pharmacokinetic parameters were determined using six animals (male Sprague-Dawley rats)/group following a single dose of 50 mg/kg by intraperitoneal injection. The analyze method was Linear Trapezoidal in A non-compartmental model using the PKsolver2.0 computer program. Data for compounds **3**, **16**, melatonin were shown as the mean  $\pm$  SD,  $n = 6$ .

<sup>b</sup>The LogP value was calculated by the free Web tool SwissADME36: <http://www.swissadme.ch/>. Lipophilicity was theoretically calculated in n-octanol buffer by the topological method.

staining results showed compounds **3** and **16** alleviated the damage of neurons. The acute toxicity results suggested the high safety of compounds **3** and **16** with the oral  $LD_{50}$  higher than 1000 mg/kg. Pharmacokinetic study showed compound **16** was prone to be absorbed into plasma and cleared than compound **3**. Compared to poor pharmacokinetic properties of melatonin featured a short plasma half-life ( $\sim 30$  min), longer plasma half-life of compounds **3** and **16** ( $13.95 \pm 4.66$  h and  $2.72 \pm 0.75$  h respectively) than melatonin supported combination strategy contributed to improved pharmacokinetic profiles. In conclusion, N-salicyloyl tryptamine derivatives were proved to be effective anti-neuroinflammatory

agents, which in turn demonstrated the combination strategy of melatonin and salicylic acid provided a new insight into multi-functional candidates for neurodegenerative diseases treatment.

## 4. Experimental

### 4.1. Chemistry

All chemicals used were of reagent grade. Proton ( $^1\text{H}$ ) and carbon ( $^{13}\text{C}$ ) NMR spectra (400 or 300 MHz for  $^1\text{H}$ NMR; 101 MHz for  $^{13}\text{C}$ NMR) were recorded on a Bruker spectrometer (Bruker Company, Germany). NMR spectra used DMSO- $d_6$ ,  $\text{CDCl}_3$  or  $\text{CH}_3\text{OD}$  as solvent (TMS as the internal standard). Proton chemical shifts are reported relative to a residual solvent peak ( $\text{CDCl}_3$  at 7.26 ppm, DMSO- $d_6$  at 2.50 ppm). Carbon chemical shifts are reported relative to a residual solvent peak ( $\text{CDCl}_3$  at 77.00 ppm, DMSO- $d_6$  at 39.60 ppm,  $\text{CH}_3\text{OD}$  at 49.03 ppm). The values of the chemical shifts are expressed in ppm and the coupling constants ( $J$ ) in hertz. The following abbreviations were used to designate multiplicities: s = singlet, d = doublet, t = triplet, q = quartet, quint = quintet, m = multiplet, br = broad. High-resolution mass spectrometry (HRMS) analysis was performed using a Bruker Daltonics Apex II 47e Specification (Bruker Company, Germany).

### 4.2. HPLC analysis

The purity was determined by high performance liquid

chromatography (HPLC). Purity of all final compounds was more than 95% (Agilent 1260 Infinity II; USA). The column was Eclipse Plus C18 (4.6 × 150 mm, 4 μm). Chromatographic conditions for most compounds except for compounds **16**, **22**, **25**, **26**, **27**: Mobile phase: 0–7 min, MeOH:H<sub>2</sub>O = 20:80; 7–16 min MeOH:H<sub>2</sub>O = 95:5, 16–25 min MeOH:H<sub>2</sub>O = 20:80; Wavelength: 254 nm; Column temperature: 25 °C; Flow rate of 0.5 mL/min. Chromatographic conditions for compounds **16**, **22**, **25**, **26**, **27**: Mobile phase: 0–15 min, MeOH:H<sub>2</sub>O = 3:97; 16–20 min MeOH:H<sub>2</sub>O = 20:80; Wavelength: 254 nm; Column temperature: 25 °C; Flow rate of 0.5 mL/min. Compounds **1** [46], **2** [46], **3** [50], **4** [51], **5** [50], **6** [48], **8** [46], **9** [44], **11** [46], **12** [46], **13** [46], **14** [46], **18** [46], **22** [49], **23** [39], **24** [47] have been previously described. Except for these compounds mentioned above, compounds **7**, **16**, **19**, **20**, **25**, **26**, **27** were not reported before.

#### 4.3. General procedure for the preparation of 1–9, 11–14, 16, 19–20, 22–27

To a solution of tryptamine derivatives (0.62 mmol) in dichloromethane (3 mL), EDCl·HCl (144 mg, 0.75 mmol) and HOBt (110 mg, 0.81 mmol), Et<sub>3</sub>N (0.22 mL, 1.56 mmol), salicylic acid derivatives (0.69 mmol) were added at room temperature and stirred for 8 h. After completion of the reaction detected by TLC, the reaction liquid was removed by rotary evaporation under reduced pressure. Then the resulting residue was purified by silica gel flash column chromatography to afford the desired product as a solid (70%–90%).

##### 4.3.1. *N*-(2-(1*H*-indol-3-yl)ethyl)-2-((3-chloro-2-methylphenyl)amino)benzamide (**1**)

Tryptamine was allowed to react with 2-((3-chloro-2-methylphenyl)amino)benzoic acid to give **1** as white solid (90% yield), mp 164–165 °C. <sup>1</sup>H NMR (400 MHz, DMSO-*d*<sub>6</sub>) δ 10.83 (s, 1H), 9.78 (s, 1H), 8.74 (t, *J* = 5.4 Hz, 1H), 7.65 (d, *J* = 7.8 Hz, 1H), 7.57 (d, *J* = 7.8 Hz, 1H), 7.37–7.23 (m, 3H), 7.23–7.11 (m, 3H), 7.06 (t, *J* = 7.5 Hz, 1H), 7.03–6.94 (m, 2H), 6.82 (t, *J* = 7.5 Hz, 1H), 3.55 (dd, *J* = 13.3, 7.0 Hz, 2H), 2.97 (t, *J* = 7.4 Hz, 2H), 2.28 (s, 3H). <sup>13</sup>C NMR (101 MHz, DMSO-*d*<sub>6</sub>) δ 168.92, 144.79, 141.65, 136.33, 134.45, 131.96, 128.81, 127.54, 127.50, 127.37, 123.23, 122.75, 121.02, 118.91, 118.62, 118.37, 118.33, 118.16, 114.98, 111.92, 111.47, 40.16, 25.06, 14.64. HRMS (ESI<sup>+</sup>) Calcd for C<sub>24</sub>H<sub>23</sub>ClN<sub>3</sub>O [M + H]<sup>+</sup> 404.1524, found 404.1528.

##### 4.3.2. *N*-(2-(1*H*-indol-3-yl)ethyl)-3-hydroxy-2-naphthamide (**2**)

Tryptamine was allowed to react with 3-hydroxy-2-naphthoic acid to give **2** as white solid (80% yield), mp 132–133 °C. <sup>1</sup>H NMR (300 MHz, DMSO-*d*<sub>6</sub>) δ 12.11 (s, 1H), 10.85 (s, 1H), 9.17 (t, *J* = 5.5 Hz, 1H), 8.50 (s, 1H), 7.84 (d, *J* = 8.1 Hz, 1H), 7.74 (d, *J* = 8.3 Hz, 1H), 7.61 (d, *J* = 7.8 Hz, 1H), 7.53–7.46 (m, 1H), 7.40–7.30 (m, 2H), 7.27 (s, 1H), 7.22 (d, *J* = 2.3 Hz, 1H), 7.11–7.04 (m, 1H), 7.03–6.96 (m, 1H), 3.65 (dd, *J* = 13.2, 7.2 Hz, 2H), 3.02 (t, *J* = 7.4 Hz, 2H). <sup>13</sup>C NMR (101 MHz, DMSO-*d*<sub>6</sub>) δ 168.18, 155.64, 136.38, 136.11, 129.54, 128.78, 128.30, 127.32, 126.67, 125.88, 123.76, 122.88, 121.09, 118.65, 118.40, 111.70, 111.53, 110.83, 40.19, 25.04. HRMS (ESI<sup>+</sup>) Calcd for C<sub>21</sub>H<sub>19</sub>N<sub>2</sub>O<sub>2</sub> [M + H]<sup>+</sup> 331.1441, found 331.1444.

##### 4.3.3. *N*-(2-(1*H*-indol-3-yl)ethyl)-2-hydroxy-4-methylbenzamide (**3**)

Tryptamine was allowed to react with 2-hydroxy-4-methylbenzoic acid to give **3** as white solid (75% yield), mp 70–71 °C. <sup>1</sup>H NMR (400 MHz, DMSO-*d*<sub>6</sub>) δ 12.73 (s, 1H), 10.83 (s, 1H), 8.87 (t, *J* = 5.4 Hz, 1H), 7.73 (d, *J* = 8.0 Hz, 1H), 7.58 (d, *J* = 7.8 Hz, 1H), 7.35 (d, *J* = 8.1 Hz, 1H), 7.18 (d, *J* = 1.6 Hz, 1H), 7.07 (t, *J* = 7.5 Hz, 1H), 6.99 (t, *J* = 7.4 Hz, 1H), 6.75–6.67 (m, 2H), 3.57 (dd, *J* = 13.5,

7.0 Hz, 2H), 2.97 (t, *J* = 7.4 Hz, 2H), 2.27 (s, 3H). <sup>13</sup>C NMR (101 MHz, DMSO-*d*<sub>6</sub>) δ 169.20, 160.45, 144.13, 136.34, 127.44, 127.29, 122.78, 121.04, 119.61, 118.36, 118.34, 117.62, 112.53, 111.70, 111.49, 39.91, 25.04, 21.16. HRMS (ESI<sup>+</sup>) Calcd for C<sub>18</sub>H<sub>19</sub>N<sub>2</sub>O<sub>2</sub> [M + H]<sup>+</sup> 295.1441, found 295.1443.

##### 4.3.4. 2-Hydroxy-*N*-(2-(5-methyl-1*H*-indol-3-yl)ethyl)benzamide (**4**)

2-(5-Methyl-1*H*-indol-3-yl)ethan-1-amine was allowed to react with salicylic acid to give **4** as white solid (75% yield), mp 170–172 °C. <sup>1</sup>H NMR (400 MHz, DMSO-*d*<sub>6</sub>) δ 12.74 (s, 1H), 10.73 (s, 1H), 8.99 (t, *J* = 5.3 Hz, 1H), 7.92–7.82 (m, 1H), 7.46–7.39 (m, 1H), 7.37 (s, 1H), 7.25 (d, *J* = 8.2 Hz, 1H), 7.17 (d, *J* = 1.7 Hz, 1H), 6.98–6.85 (m, 3H), 3.60 (dd, *J* = 13.3, 7.0 Hz, 2H), 2.98 (t, *J* = 7.3 Hz, 2H), 2.38 (s, 3H). <sup>13</sup>C NMR (101 MHz, DMSO-*d*<sub>6</sub>) δ 169.04, 160.28, 134.74, 133.71, 127.73, 127.56, 126.73, 122.93, 122.65, 118.60, 118.03, 117.49, 115.32, 111.21, 40.13, 25.02, 21.35. HRMS (ESI<sup>+</sup>) Calcd for C<sub>18</sub>H<sub>19</sub>N<sub>2</sub>O<sub>2</sub> [M + H]<sup>+</sup> 295.1441, found 295.1444.

##### 4.3.5. *N*-(2-(1*H*-indol-3-yl)ethyl)-5-chloro-2-hydroxybenzamide (**5**)

Tryptamine was allowed to react with 5-chloro-2-hydroxybenzoic acid to give **5** as white solid (70% yield), mp 171–172 °C. <sup>1</sup>H NMR (400 MHz, DMSO-*d*<sub>6</sub>) δ 12.67 (s, 1H), 10.85 (s, 1H), 9.02 (t, *J* = 5.2 Hz, 1H), 7.94 (d, *J* = 2.4 Hz, 1H), 7.58 (d, *J* = 7.8 Hz, 1H), 7.43 (dd, *J* = 8.8, 2.5 Hz, 1H), 7.35 (d, *J* = 8.0 Hz, 1H), 7.20 (s, 1H), 7.07 (t, *J* = 7.5 Hz, 1H), 7.02–6.92 (m, 2H), 3.59 (dd, *J* = 13.2, 6.9 Hz, 2H), 2.98 (t, *J* = 7.3 Hz, 2H). <sup>13</sup>C NMR (101 MHz, DMSO-*d*<sub>6</sub>) δ 167.55, 158.75, 136.36, 133.30, 127.34, 127.27, 122.88, 122.36, 121.08, 119.42, 118.39, 118.33, 116.88, 111.58, 111.52, 40.11, 24.88. HRMS (ESI<sup>+</sup>) Calcd for C<sub>17</sub>H<sub>16</sub>ClN<sub>2</sub>O<sub>2</sub> [M + H]<sup>+</sup> 315.0895, found 315.0897.

##### 4.3.6. *N*-(2-(1*H*-indol-3-yl)ethyl)-2-(methylamino)benzamide (**6**)

Tryptamine was allowed to react with 2-(methylamino)benzoic acid to give **6** as white solid (75% yield), mp 114–115 °C. <sup>1</sup>H NMR (400 MHz, DMSO-*d*<sub>6</sub>) δ 10.83 (s, 1H), 8.43 (t, *J* = 5.3 Hz, 1H), 7.70 (d, *J* = 4.9 Hz, 1H), 7.59 (d, *J* = 7.8 Hz, 1H), 7.52 (d, *J* = 7.8 Hz, 1H), 7.35 (d, *J* = 8.0 Hz, 1H), 7.28 (t, *J* = 7.7 Hz, 1H), 7.18 (s, 1H), 7.07 (t, *J* = 7.4 Hz, 1H), 6.99 (t, *J* = 7.3 Hz, 1H), 6.62 (d, *J* = 8.3 Hz, 1H), 6.55 (t, *J* = 7.4 Hz, 1H), 3.50 (dd, *J* = 13.6, 7.0 Hz, 2H), 2.94 (t, *J* = 7.5 Hz, 2H), 2.77 (d, *J* = 5.0 Hz, 3H). <sup>13</sup>C NMR (101 MHz, DMSO-*d*<sub>6</sub>) δ 169.16, 150.18, 136.34, 132.33, 128.23, 127.38, 122.69, 121.02, 118.42, 118.32, 115.35, 113.97, 112.03, 111.48, 110.55, 39.96, 29.38, 25.29. HRMS (ESI<sup>+</sup>) Calcd for C<sub>18</sub>H<sub>20</sub>N<sub>3</sub>O [M + H]<sup>+</sup> 294.1601, found 294.1605.

##### 4.3.7. *N*-(2-(1*H*-indol-3-yl)ethyl)-2,4-dihydroxybenzamide (**7**)

Tryptamine was allowed to react with 2,4-dihydroxybenzoic acid to give **7** as white solid (65% yield), mp 168–169 °C. <sup>1</sup>H NMR (400 MHz, DMSO-*d*<sub>6</sub>) δ 13.00 (s, 1H), 10.81 (s, 1H), 10.04 (s, 1H), 8.67 (t, *J* = 5.6 Hz, 1H), 7.68 (d, *J* = 8.8 Hz, 1H), 7.58 (d, *J* = 7.8 Hz, 1H), 7.35 (d, *J* = 8.1 Hz, 1H), 7.18 (d, *J* = 2.2 Hz, 1H), 7.11–7.05 (m, 1H), 7.02–6.96 (m, 1H), 6.30 (dd, *J* = 8.7, 2.4 Hz, 1H), 6.25 (d, *J* = 2.4 Hz, 1H), 3.55 (dd, *J* = 13.4, 7.2 Hz, 2H), 2.96 (t, *J* = 7.5 Hz, 2H). <sup>13</sup>C NMR (101 MHz, DMSO-*d*<sub>6</sub>) δ 169.43, 162.67, 162.24, 136.34, 128.96, 127.31, 122.73, 121.03, 118.34, 111.78, 111.47, 107.01, 106.83, 102.83, 40.28, 25.15. HRMS (ESI<sup>+</sup>) Calcd for C<sub>17</sub>H<sub>17</sub>N<sub>2</sub>O<sub>3</sub> [M + H]<sup>+</sup> 297.1234, found 297.1238.

##### 4.3.8. *N*-(2-(5-methyl-1*H*-indol-3-yl)ethyl)-2-(phenylamino)benzamide (**8**)

2-(5-Methyl-1*H*-indol-3-yl)ethan-1-amine was allowed to react with 2-(phenylamino)benzoic acid to give **8** as white solid (90% yield), mp 176–177 °C. <sup>1</sup>H NMR (400 MHz, DMSO-*d*<sub>6</sub>) δ 10.69 (s, 1H), 9.75 (s, 1H), 8.68 (t, *J* = 5.1 Hz, 1H), 7.63 (d, *J* = 8.0 Hz, 1H), 7.37–7.27 (m, 5H), 7.22 (d, *J* = 8.2 Hz, 1H), 7.20–7.10 (m, 3H), 6.97 (t, *J* = 7.3 Hz,

1H), 6.89 (d, *J* = 8.2 Hz, 1H), 6.85–6.77 (m, 1H), 3.52 (dd, *J* = 13.0, 6.9 Hz, 2H), 2.93 (t, *J* = 7.2 Hz, 2H), 2.36 (s, 3H). <sup>13</sup>C NMR (101 MHz, DMSO-*d*<sub>6</sub>) δ 168.82, 144.33, 141.64, 134.73, 131.85, 129.50, 128.89, 127.62, 126.69, 122.85, 122.62, 121.80, 119.50, 119.07, 118.13, 118.05, 114.99, 111.46, 111.19, 40.23, 25.12, 21.38. HRMS (ESI+) Calcd for C<sub>24</sub>H<sub>24</sub>N<sub>3</sub>O [M + H]<sup>+</sup> 370.1914, found 370.1917.

#### 4.3.9. 2-Hydroxy-*N*-(2-(5-hydroxy-1*H*-indol-3-yl)ethyl)benzamide (**9**)

5-Hydroxytryptamine was allowed to react with salicylic acid to give **9** as white solid (40% yield), mp 140–141 °C. <sup>1</sup>H NMR (400 MHz, DMSO-*d*<sub>6</sub>) δ 12.73 (s, 1H), 10.52 (d, *J* = 1.5 Hz, 1H), 8.96 (t, *J* = 5.6 Hz, 1H), 8.62 (s, 1H), 7.85 (dd, *J* = 7.9, 1.4 Hz, 1H), 7.43–7.36 (m, 1H), 7.13 (d, *J* = 8.6 Hz, 1H), 7.08 (d, *J* = 2.2 Hz, 1H), 6.92–6.85 (m, 3H), 6.61 (dd, *J* = 8.6, 2.3 Hz, 1H), 3.55 (dd, *J* = 14.4, 6.4 Hz, 2H), 2.88 (t, *J* = 7.5 Hz, 2H). <sup>13</sup>C NMR (101 MHz, DMSO-*d*<sub>6</sub>) δ 169.04, 160.29, 150.33, 133.71, 130.93, 127.96, 127.69, 123.24, 118.60, 117.49, 115.29, 111.79, 111.44, 110.67, 102.33, 40.28, 25.18. HRMS (ESI+) Calcd for C<sub>17</sub>H<sub>17</sub>N<sub>2</sub>O<sub>3</sub> [M + H]<sup>+</sup> 297.1234, found 297.1238.

#### 4.3.10. *N*-(2-(1*H*-indol-3-yl)ethyl)-2-hydroxy-5-methylbenzamide (**11**)

Tryptamine was allowed to react with 2-hydroxy-5-methylbenzoic acid to give **11** as white solid (75% yield), mp 153–154 °C. <sup>1</sup>H NMR (400 MHz, DMSO-*d*<sub>6</sub>) δ 12.43 (s, 1H), 10.84 (s, 1H), 8.90 (t, *J* = 5.1 Hz, 1H), 7.67 (s, 1H), 7.59 (d, *J* = 7.8 Hz, 1H), 7.35 (d, *J* = 8.0 Hz, 1H), 7.20 (m, 2H), 7.08 (t, *J* = 7.4 Hz, 1H), 6.99 (t, *J* = 7.4 Hz, 1H), 6.80 (d, *J* = 8.3 Hz, 1H), 3.59 (dd, *J* = 13.4, 6.9 Hz, 2H), 2.98 (t, *J* = 7.4 Hz, 2H), 2.24 (s, 3H). <sup>13</sup>C NMR (101 MHz, DMSO-*d*<sub>6</sub>) δ 169.04, 157.99, 136.36, 134.33, 127.62, 127.30, 127.17, 122.78, 121.05, 118.36, 118.35, 117.25, 114.93, 111.70, 111.50, 39.94, 25.03, 20.18. HRMS (ESI+) Calcd for C<sub>18</sub>H<sub>19</sub>N<sub>2</sub>O<sub>2</sub> [M + H]<sup>+</sup> 295.1441, found 295.1445.

#### 4.3.11. *N*-(2-(1*H*-indol-3-yl)ethyl)-4-fluoro-2-hydroxybenzamide (**12**)

Tryptamine was allowed to react with 4-fluoro-2-hydroxybenzoic acid to give **12** as white solid (75% yield), mp 146–147 °C. <sup>1</sup>H NMR (400 MHz, DMSO-*d*<sub>6</sub>) δ 13.21 (s, 1H), 10.85 (s, 1H), 9.07–8.93 (m, 1H), 7.98–7.91 (m, 1H), 7.58 (d, *J* = 7.8 Hz, 1H), 7.35 (d, *J* = 8.1 Hz, 1H), 7.19 (d, *J* = 2.3 Hz, 1H), 7.10–7.04 (m, 1H), 7.01–6.95 (m, 1H), 6.79–6.72 (m, 2H), 3.58 (dd, *J* = 13.3, 7.3 Hz, 2H), 2.98 (t, *J* = 7.4 Hz, 2H). <sup>13</sup>C NMR (101 MHz, DMSO-*d*<sub>6</sub>) δ 168.39, 165.07 (d, *J* = 249.4 Hz), 162.45 (d, *J* = 13.4 Hz), 136.35, 130.03 (d, *J* = 11.1 Hz), 127.27, 122.82, 121.05, 118.37, 118.31, 112.26 (d, *J* = 2.5 Hz), 111.61, 111.50, 106.16 (d, *J* = 22.1 Hz), 104.00 (d, *J* = 23.5 Hz), 40.28, 24.95. HRMS (ESI+) Calcd for C<sub>17</sub>H<sub>16</sub>FN<sub>2</sub>O<sub>2</sub> [M + H]<sup>+</sup> 299.1190, found 299.1194.

#### 4.3.12. *N*-(2-(1*H*-indol-3-yl)ethyl)-2-(phenylamino)benzamide (**13**)

Tryptamine was allowed to react with 2-(phenylamino)benzoic acid to give **13** as white solid (75% yield), mp 174–175 °C. <sup>1</sup>H NMR (400 MHz, DMSO-*d*<sub>6</sub>) δ 10.83 (s, 1H), 9.74 (s, 1H), 8.70 (t, *J* = 5.4 Hz, 1H), 7.63 (d, *J* = 8.0 Hz, 1H), 7.58 (d, *J* = 7.8 Hz, 1H), 7.38–7.25 (m, 5H), 7.21–7.13 (m, 3H), 7.07 (t, *J* = 7.5 Hz, 1H), 7.01–6.93 (m, 2H), 6.85–6.78 (m, 1H), 3.54 (dd, *J* = 13.5, 6.9 Hz, 2H), 2.96 (t, *J* = 7.4 Hz, 2H). <sup>13</sup>C NMR (101 MHz, DMSO-*d*<sub>6</sub>) δ 168.85, 144.31, 141.65, 136.34, 131.85, 129.50, 128.88, 127.37, 122.74, 121.80, 121.03, 119.48, 119.11, 118.39, 118.34, 118.15, 115.03, 111.93, 111.48, 40.17, 25.11. HRMS (ESI+) Calcd for C<sub>23</sub>H<sub>22</sub>N<sub>3</sub>O [M + H]<sup>+</sup> 356.1757, found 356.1753.

#### 4.3.13. *N*-(2-(5-methoxy-1*H*-indol-3-yl)ethyl)-2-(phenylamino)benzamide (**14**)

2-(5-Methoxy-1*H*-indol-3-yl)ethan-1-amine was allowed to

react with 2-(phenylamino)benzoic acid to give **14** as white solid (75% yield), mp 121–122 °C. <sup>1</sup>H NMR (400 MHz, DMSO-*d*<sub>6</sub>) δ 10.67 (s, 1H), 9.77 (s, 1H), 8.69 (t, *J* = 5.4 Hz, 1H), 7.63 (d, *J* = 8.0 Hz, 1H), 7.37–7.26 (m, 4H), 7.23 (d, *J* = 8.7 Hz, 1H), 7.15 (d, *J* = 6.7 Hz, 3H), 7.07 (d, *J* = 2.0 Hz, 1H), 6.97 (t, *J* = 7.3 Hz, 1H), 6.85–6.77 (m, 1H), 6.71 (dd, *J* = 8.7, 2.2 Hz, 1H), 3.73 (s, 3H), 3.53 (dd, *J* = 13.2, 6.8 Hz, 2H), 2.92 (t, *J* = 7.3 Hz, 2H). <sup>13</sup>C NMR (101 MHz, DMSO-*d*<sub>6</sub>) δ 168.85, 153.08, 144.35, 141.63, 131.88, 131.47, 129.51, 128.89, 127.71, 123.41, 121.80, 119.47, 118.99, 118.13, 114.99, 112.12, 111.79, 111.19, 100.22, 55.35, 40.14, 25.12. HRMS (ESI+) Calcd for C<sub>24</sub>H<sub>24</sub>N<sub>3</sub>O<sub>2</sub> [M + H]<sup>+</sup> 386.1863, found 386.1866.

#### 4.3.14. *N*-(2-(5-hydroxy-1*H*-indol-3-yl)ethyl)-2-(phenylamino)benzamide (**16**)

5-Hydroxytryptamine was allowed to react with 2-(phenylamino)benzoic acid to give **16** as white solid (75% yield), mp 131–133 °C. <sup>1</sup>H NMR (400 MHz, DMSO-*d*<sub>6</sub>) δ 10.54 (s, 1H), 9.78 (s, 1H), 8.72 (t, *J* = 5.3 Hz, 1H), 8.66 (s, 1H), 7.68 (d, *J* = 7.9 Hz, 1H), 7.34 (t, *J* = 7.6 Hz, 4H), 7.18 (dd, *J* = 11.1, 8.4 Hz, 3H), 7.12 (s, 1H), 7.00 (t, *J* = 7.3 Hz, 1H), 6.93 (s, 1H), 6.89–6.83 (m, 1H), 6.64 (dd, *J* = 8.6, 2.0 Hz, 1H), 3.53 (dd, *J* = 13.6, 6.8 Hz, 2H), 2.89 (t, *J* = 7.5 Hz, 2H). <sup>13</sup>C NMR (101 MHz, MeOD) δ 171.60, 151.11, 145.69, 143.39, 133.09, 132.90, 130.33, 129.72, 129.44, 124.30, 123.07, 121.45, 120.85, 119.77, 116.91, 112.72, 112.56, 112.40, 103.62, 41.57, 26.28. HRMS (ESI+) Calcd for C<sub>23</sub>H<sub>22</sub>N<sub>3</sub>O<sub>2</sub> [M + H]<sup>+</sup> 372.1707, found 372.1704.

#### 4.3.15. *N*-(2-(5-chloro-1*H*-indol-3-yl)ethyl)-2-(phenylamino)benzamide (**18**)

2-(5-Chloro-1*H*-indol-3-yl)ethan-1-amine was allowed to react with 2-(phenylamino)benzoic acid to give **18** as white solid (75% yield), mp 156–157 °C. <sup>1</sup>H NMR (400 MHz, DMSO-*d*<sub>6</sub>) δ 11.05 (s, 1H), 9.71 (s, 1H), 8.68 (t, *J* = 5.1 Hz, 1H), 7.67–7.54 (m, 2H), 7.40–7.23 (m, 6H), 7.15 (d, *J* = 7.9 Hz, 2H), 7.06 (d, *J* = 8.6 Hz, 1H), 6.96 (t, *J* = 7.2 Hz, 1H), 6.82 (t, *J* = 6.9 Hz, 1H), 3.51 (dd, *J* = 13.1, 6.7 Hz, 2H), 2.93 (t, *J* = 7.2 Hz, 2H). <sup>13</sup>C NMR (101 MHz, DMSO-*d*<sub>6</sub>) δ 168.84, 144.32, 141.63, 134.79, 131.87, 129.49, 128.85, 128.56, 124.76, 123.12, 121.81, 120.95, 119.51, 119.04, 118.16, 117.72, 115.01, 113.02, 111.99, 40.11, 24.88. HRMS (ESI+) Calcd for C<sub>23</sub>H<sub>21</sub>ClN<sub>3</sub>O [M + H]<sup>+</sup> 390.1368, found 390.1371.

#### 4.3.16. 2-((3-chloro-2-methylphenyl)amino)-*N*-(2-(5-methyl-1*H*-indol-3-yl)ethyl)-benzamide (**19**)

2-(5-Methyl-1*H*-indol-3-yl)ethan-1-amine was allowed to react with 2-((3-chloro-2-methylphenyl)amino)benzoic acid to give **19** as white solid (90% yield), mp 145–147 °C. <sup>1</sup>H NMR (400 MHz, DMSO-*d*<sub>6</sub>) δ 10.68 (s, 1H), 9.80 (s, 1H), 8.73 (t, *J* = 5.6 Hz, 1H), 7.65 (dd, *J* = 7.9, 1.4 Hz, 1H), 7.35 (s, 1H), 7.33–7.28 (m, 1H), 7.26 (dd, *J* = 7.9, 1.1 Hz, 1H), 7.21 (d, *J* = 8.2 Hz, 1H), 7.18 (t, *J* = 7.9 Hz, 1H), 7.12 (dd, *J* = 7.9, 1.2 Hz, 2H), 7.01 (d, *J* = 7.6 Hz, 1H), 6.88 (dd, *J* = 8.3, 1.4 Hz, 1H), 6.85–6.79 (m, 1H), 3.52 (dd, *J* = 13.3, 7.1 Hz, 2H), 2.92 (t, *J* = 7.4 Hz, 2H), 2.35 (s, 3H), 2.27 (s, 3H). <sup>13</sup>C NMR (101 MHz, DMSO-*d*<sub>6</sub>) δ 168.88, 144.79, 141.66, 134.72, 134.44, 131.96, 128.80, 127.61, 127.51, 127.49, 126.67, 123.22, 122.83, 122.60, 118.89, 118.60, 118.16, 118.04, 114.97, 111.44, 111.17, 40.26, 25.08, 21.36, 14.62. HRMS (ESI+) Calcd for C<sub>25</sub>H<sub>25</sub>ClN<sub>3</sub>O [M + H]<sup>+</sup> 418.1681, found 418.1685.

#### 4.3.17. 2-((3-chloro-2-methylphenyl)amino)-*N*-(2-(5-methoxy-1*H*-indol-3-yl)ethyl)-benzamide (**20**)

2-(5-Methoxy-1*H*-indol-3-yl)ethan-1-amine was allowed to react with 2-((3-chloro-2-methylphenyl)amino)benzoic acid to give **20** as white solid (85% yield), mp 177–178 °C. <sup>1</sup>H NMR (400 MHz, DMSO-*d*<sub>6</sub>) δ 10.66 (s, 1H), 9.82 (s, 1H), 8.74 (t, *J* = 5.4 Hz, 1H), 7.66 (d, *J* = 7.9 Hz, 1H), 7.34–7.20 (m, 3H), 7.15 (p, *J* = 7.9 Hz, 3H), 7.08 (d, *J* = 2.0 Hz, 1H), 7.02 (d, *J* = 8.3 Hz, 1H), 6.82 (t, *J* = 7.5 Hz, 1H), 6.71 (dd, *J* = 8.7, 2.2 Hz, 1H), 3.73 (s, 3H), 3.54 (dd, *J* = 13.2,

6.9 Hz, 2H), 2.93 (t,  $J = 7.3$  Hz, 2H), 2.27 (s, 3H).  $^{13}\text{C NMR}$  (101 MHz, DMSO- $d_6$ )  $\delta$  168.92, 153.07, 144.80, 141.63, 134.44, 131.99, 131.46, 128.82, 127.70, 127.49, 127.45, 123.41, 123.19, 118.82, 118.51, 118.14, 114.94, 112.11, 111.76, 111.20, 100.19, 55.31, 40.13, 25.12, 14.59. HRMS (ESI+) Calcd for  $\text{C}_{25}\text{H}_{25}\text{ClN}_3\text{O}_2$   $[\text{M} + \text{H}]^+$  434.1630, found 434.1634.

#### 4.3.18. *N*-(2-(1*H*-indol-3-yl)ethyl)-2-((2,3-dimethylphenyl)amino)benzamide (**22**)

Tryptamine was allowed to react with 2-((2,3-dimethylphenyl)amino)benzoic acid to give **22** as white solid (85% yield), mp 143–145 °C.  $^1\text{H NMR}$  (400 MHz, DMSO- $d_6$ )  $\delta$  10.85 (s, 1H), 9.66 (s, 1H), 8.69 (t,  $J = 5.6$  Hz, 1H), 7.66–7.57 (m, 2H), 7.35 (d,  $J = 8.1$  Hz, 1H), 7.26–7.20 (m, 2H), 7.13–7.04 (m, 3H), 7.01–6.96 (m, 1H), 6.92 (d,  $J = 7.0$  Hz, 1H), 6.87–6.83 (m, 1H), 6.75–6.70 (m, 1H), 3.57 (dd,  $J = 13.4, 7.1$  Hz, 2H), 2.99 (t,  $J = 7.4$  Hz, 2H), 2.27 (s, 3H), 2.12 (s, 3H).  $^{13}\text{C NMR}$  (101 MHz, DMSO- $d_6$ )  $\delta$  169.17, 146.28, 139.45, 137.78, 136.36, 131.93, 129.47, 128.72, 127.41, 125.96, 125.13, 122.76, 121.04, 119.75, 118.42, 118.36, 117.39, 116.85, 114.02, 112.00, 111.50, 40.16, 25.16, 20.42, 13.70. HRMS (ESI+) Calcd for  $\text{C}_{25}\text{H}_{26}\text{N}_3\text{O}$   $[\text{M} + \text{H}]^+$  370.1914, found 370.1918.

#### 4.3.19. *N*-(2-(1*H*-indol-3-yl)ethyl)-2-hydroxybenzamide (**23**)

Tryptamine was allowed to react with 2-hydroxybenzoic acid to give **23** as white solid (80% yield), mp 153–155 °C.  $^1\text{H NMR}$  (400 MHz, DMSO- $d_6$ )  $\delta$  12.71 (s, 1H), 10.84 (s, 1H), 8.98 (t,  $J = 5.6$  Hz, 1H), 7.85 (dd,  $J = 7.9, 1.5$  Hz, 1H), 7.59 (d,  $J = 7.8$  Hz, 1H), 7.42–7.32 (m, 2H), 7.20 (d,  $J = 2.2$  Hz, 1H), 7.10–7.04 (m, 1H), 7.02–6.96 (m, 1H), 6.92–6.85 (m, 2H), 3.59 (dd,  $J = 13.9, 6.7$  Hz, 2H), 2.99 (t,  $J = 7.4$  Hz, 2H).  $^{13}\text{C NMR}$  (101 MHz, DMSO- $d_6$ )  $\delta$  168.98, 160.21, 136.32, 133.64, 127.68, 127.26, 122.75, 121.00, 118.54, 118.32, 118.29, 117.43, 115.31, 111.65, 111.45, 39.94, 24.97. HRMS (ESI+) Calcd for  $\text{C}_{17}\text{H}_{17}\text{N}_2\text{O}_2$   $[\text{M} + \text{H}]^+$  281.1285, found 281.1289.

#### 4.3.20. *N*-(2-(1*H*-indol-3-yl)ethyl)-2-(dimethylamino)benzamide (**24**)

Tryptamine was allowed to react with 2-(dimethylamino)benzoic acid to give **24** as white solid (50% yield), mp 167–169 °C.  $^1\text{H NMR}$  (400 MHz, DMSO- $d_6$ )  $\delta$  10.88 (s, 1H), 9.13 (t,  $J = 5.2$  Hz, 1H), 7.66 (dd,  $J = 7.7, 1.7$  Hz, 1H), 7.60 (d,  $J = 7.8$  Hz, 1H), 7.39–7.32 (m, 2H), 7.23 (d,  $J = 2.2$  Hz, 1H), 7.13–7.06 (m, 2H), 7.06–7.01 (m, 1H), 7.01–6.96 (m, 1H), 3.62 (dd,  $J = 12.7, 7.0$  Hz, 2H), 2.97 (t,  $J = 7.1$  Hz, 2H), 2.45 (s, 6H).  $^{13}\text{C NMR}$  (101 MHz, DMSO- $d_6$ )  $\delta$  166.71, 151.58, 136.45, 131.17, 130.08, 127.72, 127.28, 123.01, 122.05, 121.07, 118.87, 118.45, 118.35, 111.77, 111.47, 43.94, 39.66, 24.84. HRMS (ESI+) Calcd for  $\text{C}_{19}\text{H}_{22}\text{N}_3\text{O}$   $[\text{M} + \text{H}]^+$  308.1757, found 308.1753.

#### 4.3.21. 2-((2,3-dimethylphenyl)amino)-*N*-(2-(5-hydroxy-1*H*-indol-3-yl)ethyl)benzamide (**25**)

5-Hydroxytryptamine was allowed to react with 2-((2,3-dimethylphenyl)amino)benzoic acid to give **25** as white solid (75% yield), mp 139–140 °C.  $^1\text{H NMR}$  (400 MHz, DMSO- $d_6$ )  $\delta$  10.49 (d,  $J = 1.6$  Hz, 1H), 9.62 (s, 1H), 8.64 (t,  $J = 5.6$  Hz, 1H), 8.60 (s, 1H), 7.64 (dd,  $J = 7.9, 1.3$  Hz, 1H), 7.26–7.20 (m, 1H), 7.15–7.04 (m, 4H), 6.94–6.89 (m, 2H), 6.85–6.81 (m, 1H), 6.75–6.70 (m, 1H), 6.61 (dd,  $J = 8.6, 2.3$  Hz, 1H), 3.52 (dd,  $J = 14.4, 6.4$  Hz, 2H), 2.93–2.84 (m, 2H), 2.27 (s, 3H), 2.12 (s, 3H).  $^{13}\text{C NMR}$  (101 MHz, DMSO- $d_6$ )  $\delta$  169.09, 150.30, 146.31, 139.43, 137.76, 131.90, 130.94, 129.56, 128.68, 128.02, 125.94, 125.17, 123.17, 119.88, 117.35, 116.83, 113.97, 111.76, 111.40, 110.96, 102.39, 39.92, 25.32, 20.37, 13.68. HRMS (ESI+) Calcd for  $\text{C}_{25}\text{H}_{26}\text{N}_3\text{O}_2$   $[\text{M} + \text{H}]^+$  400.2020, found 400.2024.

#### 4.3.22. *N*-(2-(1*H*-indol-3-yl)ethyl)-2-(methyl(phenyl)amino)benzamide (**26**)

Tryptamine was allowed to react with 2-(methyl(phenyl)amino)benzoic acid to give **26** as white solid (50% yield), mp 103–105 °C.

$^1\text{H NMR}$  (400 MHz,  $\text{CDCl}_3$ )  $\delta$  8.37–8.26 (m, 1H), 8.23 (dd,  $J = 7.8, 1.7$  Hz, 1H), 7.65 (d,  $J = 8.2$  Hz, 1H), 7.56 (d,  $J = 7.9$  Hz, 1H), 7.39 (td,  $J = 7.6, 1.8$  Hz, 1H), 7.35–7.26 (m, 2H), 7.25–7.15 (m, 3H), 7.12–7.06 (m, 1H), 7.00 (dd,  $J = 7.8, 1.1$  Hz, 1H), 6.93 (t, 1H), 6.65–6.52 (m,  $J = 5.2$  Hz, 3H), 3.80 (dd,  $J = 12.0, 6.5$  Hz, 2H), 2.94 (t,  $J = 6.6$  Hz, 2H), 2.71 (s, 3H).  $^{13}\text{C NMR}$  (101 MHz,  $\text{CDCl}_3$ )  $\delta$  165.71, 149.12, 148.13, 136.45, 132.44, 131.45, 130.94, 128.95, 127.72, 126.95, 126.53, 122.37, 122.01, 119.74, 119.27, 118.74, 116.27, 112.44, 111.23, 40.24, 39.32, 24.87. HRMS (ESI+) Calcd for  $\text{C}_{24}\text{H}_{24}\text{N}_3\text{O}$   $[\text{M} + \text{H}]^+$  370.1914, found 370.1918.

#### 4.3.23. 2-amino-*N*-(2-(5-hydroxy-1*H*-indol-3-yl)ethyl)benzamide (**27**)

5-Hydroxytryptamine was allowed to react with 2-(dimethylamino)benzoic acid to give **27** as white solid (30% yield), mp 150–151 °C.  $^1\text{H NMR}$  (400 MHz, DMSO- $d_6$ )  $\delta$  10.57 (s, 1H), 9.12 (t,  $J = 4.8$  Hz, 1H), 8.62 (d,  $J = 1.7$  Hz, 1H), 7.68–7.63 (m, 1H), 7.38–7.32 (m, 1H), 7.17–7.09 (m, 3H), 7.03 (td,  $J = 7.5, 1.0$  Hz, 1H), 6.92–6.88 (m, 1H), 6.61 (dt,  $J = 8.6, 1.9$  Hz, 1H), 3.58 (dd,  $J = 12.7, 6.1$  Hz, 2H), 2.88 (t,  $J = 7.1$  Hz, 2H), 2.46 (s, 6H).  $^{13}\text{C NMR}$  (101 MHz, MeOD)  $\delta$  169.34, 154.09, 151.36, 133.27, 133.22, 131.51, 129.44, 128.15, 124.72, 124.58, 120.96, 112.85, 112.61, 112.31, 103.61, 44.82, 41.01, 25.69. HRMS (ESI+) Calcd for  $\text{C}_{19}\text{H}_{22}\text{N}_3\text{O}_2$   $[\text{M} + \text{H}]^+$  324.1707, found 324.1709.

### 4.4. Biological studies

#### 4.4.1. COX inhibition assay

The COX-1 and COX-2 inhibitory activities of the compounds were measured using human COX inhibitory screening assay kit (Cayman Chemical, catalog no. 701230) according to the manufacturer's instructions. The final concentrations of compounds were 2.5, 5, 10, 20, 40  $\mu\text{M}$ . The absorbance was measured in microplate reader (Bio-Rad Laboratories, CA, USA) at 405 nm.  $\text{IC}_{50}$  values were calculated by the sigmoidal dose–response equation (variable slope) (GraphPad software). All the experiments were repeated three times.

#### 4.4.2. Cells and treatment

BV2 and C6 cell lines were obtained from the American Type Culture Collection (ATCC, USA). Both BV2 and C6 cell lines were incubated in DMEM media supplemented with 10% FBS, 100 U/mL penicillin, and 100 U/mL streptomycin at 37 °C with 5%  $\text{CO}_2$ . Compounds dissolved in DMSO solution were added into cell culture medium with the final concentration of DMSO less than 0.4%.

#### 4.4.3. Cytotoxicity assay on C6 and BV2 cells

In order to evaluate the cytotoxicity of all the compounds on C6 and BV2 cells, MTT assay was performed. To be specific, the cells were collected after being dissociated by trypsin, and seeded in 96 well plate at the density of  $1-5 \times 10^5$  per well. After 12 h, the medium was changed, and the cells were treated by the medium containing compounds at final concentrations of 0, 6.25, 12.5, 25, 50, and 100  $\mu\text{M}$  for 24h followed by incubation with MTT solution for 4 h. After adding 100  $\mu\text{L}$  of DMSO per well, the absorbance was measured in microplate reader (Bio-Rad Laboratories, CA, USA) at 570 nm.  $\text{IC}_{50}$  values were calculated by IBM SPSS Statistics 25.0. Data were given as the mean from three independent experiments conducted in triplicate.

#### 4.4.4. Evaluation of LPS-induced NO production in C6 and BV2 cells models

The C6 and BV2 cells in logarithmic growth period were collected after being dissociated by trypsin and then seeded in 96-well plates at a density of  $5 \times 10^5$  cells/mL. 12 h after attachment,

the BV2 and C6 cells were stimulated by LPS (Solarbio, Lot.L8880, China) at 1 and 10  $\mu\text{g}/\text{mL}$  respectively. The cells in treatment group were incubated with compounds at the final concentrations of 2.5, 5, 10, 20, 40  $\mu\text{M}$  while in blank group, equal volume of DMSO was added. After 24 h incubation, supernatant was collected. The production of nitric oxide was quantified using the Griess reagent (0.5% sulfanilamide, 0.05% (N-1-naphthyl) ethylenediamine dihydrochloride, 2.5%  $\text{H}_3\text{PO}_4$ ) for 15 min at rt in the dark. The absorbance was measured at 540 nm in microplate reader (Bio-Rad Laboratories, CA, USA). The concentration of nitrite was determined according to a sodium nitrite standard curve.  $\text{IC}_{50}$  values were calculated by IBM SPSS Statistics 25.0. All the experiments were repeated three times.

#### 4.4.5. Evaluation on TNF- $\alpha$ , IL-10, and PGE<sub>2</sub> in LPS-induced activation of C6 and BV2 cells model

The C6 and BV2 cells in logarithmic growth period were collected after being dissociated by trypsin and then dispensed in 96-well plates at a density of  $5 \times 10^5$  cells/mL. About 12 h after attachment, the BV2 and C6 cells were respectively stimulated by LPS (Solarbio, Lot.L8880, China) at 1 and 10  $\mu\text{g}/\text{mL}$ . The cells in treatment group were treated with compounds at the final concentrations of 10, 20, 40  $\mu\text{M}$  while in blank group, equal volume of DMSO was added. After 24 h, secreted TNF- $\alpha$ , IL-10, PGE<sub>2</sub> in the supernatant of culture media were measured using the specific ELISA kit (TNF- $\alpha$ : Elabscience, E-EL-M0049c; IL-10: Elabscience, E-EL-M0046c; PGE<sub>2</sub>: Elabscience, E-EL-0034c) according to the manufacturer's instructions. In detail, for TNF- $\alpha$  and IL-10 measurements, standards or samples were added into micro ELISA plate wells. Then specific antibodies of biotinylated detection for Mouse TNF- $\alpha$ , IL-10, Avidin-Horseradish Peroxidase (HRP) conjugate were added into each well and incubated. The reaction was terminated by adding stop solution with the sign of color turning to yellow. The optical density (OD) was measured spectrophotometrically at a wavelength of  $450 \pm 2$  nm. The OD value was proportional to the concentration of mouse TNF- $\alpha$ , IL-10. And LPS was used to set up a positive control. The absorbance was measured by a microplate reader (Bio-Rad Laboratories, CA, USA). Besides, for PGE<sub>2</sub> measurement, the ELISA kit worked based on the competitive-ELISA principle. The micro ELISA plate provided in this kit had been pre-coated with a certain amount of PGE<sub>2</sub>. During the reaction, PGE<sub>2</sub> in the sample or standard competed with the fixed amount of PGE<sub>2</sub> on the solid phase supporter for binding sites of Biotinylated Detection Ab specific to PGE<sub>2</sub>. Unbonded conjugate and excess sample or standard were washed from the plate, and Avidin conjugated to Horseradish Peroxidase (HRP) were added to each microplate well and incubated. Then a TMB substrate solution was added into each well. The enzyme-substrate reaction was terminated by adding stop solution and the intensity of changed color was measured spectrophotometrically at a wavelength of  $450 \pm 2$  nm by a microplate reader (Bio-Rad Laboratories, CA, USA). The concentration of PGE<sub>2</sub> in the samples were then determined by comparing the OD of the samples to the standard curve. The results were calculated from at least three independent experiments.

#### 4.4.6. Evaluation of inhibition on LPS-induced expression of iNOS and COX-2 in C6 and BV2 cells models

C6 and BV2 cells were seeded into 6-well plates at a density of  $5 \times 10^5$  cells/mL with 2 mL of culture medium and incubated in incubator (5%  $\text{CO}_2$ , 37 °C) overnight. After attachment, they were divided into control group, LPS treated group and LPS + compound treated group. In LPS + compound treated group, each compound at final concentrations of 10, 20, 40  $\mu\text{M}$  were added. At the same time, equal volume of DMSO was added into LPS treated group and blank group. LPS (Solarbio, Lot.L8880, China) of 10  $\mu\text{g}/\text{mL}$  and 1  $\mu\text{g}/$

mL were respectively added in C6 and BV2 apart from blank group. After incubation for 24 h, cells were collected after washing with ice-cold phosphate buffered saline (PBS) for three times. Then the collected cells were lysed in 300  $\mu\text{L}$  RIPA lysis buffer (Solarbio, R0010, China) containing 1 mM phenylmethanesulfonyl fluoride (PMSF: Solarbio, R0010, China) for 10 min, followed by centrifugation at 12000 rpm for 10 min at 4 °C. The protein concentrations were determined by BCA protein assay kit (Solarbio, PC0020, China). Equal amounts of proteins (30  $\mu\text{g}$ ) were separated by 8% SDS-PAGE gels and transferred to polyvinylidene difluoride (PVDF) membranes (Millipore Corporation, USA). The non-objective protein was blocked in blocking buffer (5% non-fat dry milk in TBST) for 2 h at room temperature. After that, the membranes were incubated with the diluted (1:500–1:1000) iNOS antibodies (Affinity Biosciences, USA, Lot. AF0199) and COX-2 antibodies (Cell Signaling Technology, Inc., USA, Lot. 4842) overnight at 4 °C, followed by washing with TBST at least three times. And then, the membranes were incubated with HRP-coupled antibody (Affinity Biosciences, USA, Lot. S0001 for iNOS and COX-2; Affinity Biosciences, USA, Lot. S0002 for GAPDH) at 1:5000 dilution in blocking buffer for 2 h at room temperature. After washing with TBST at least three times, the immunocomplexes were detected using ECL reagent (Millipore, Billerica, MA) and scanned using the Tanon imaging system (Tanon Science & Technology Co., Ltd, China). All the images were quantified by densitometry using Image J software. The results were calculated from at least three independent experiments.

#### 4.4.7. Evaluation on LPS-induced ROS production in BV2 cells model

BV2 cells were seeded into 6-well plates at a density of  $5 \times 10^5$  cells/mL with 2 mL of culture medium and incubated in incubator (5%  $\text{CO}_2$ , 37 °C) overnight. After attachment, they were divided into control group, LPS treated group and LPS + compound treated group. In LPS + compound treated group, compounds at final concentrations of 10, 20, 40  $\mu\text{M}$  were added. At the same time, equal volume of DMSO was added into LPS treated group and blank group, and LPS (Solarbio, Lot.L8880, China) of 1  $\mu\text{g}/\text{mL}$  were added apart from blank group. After incubation for 6 h, the growth media were removed, and carboxy-21,71-dichloro-dihydro-fluorescein diacetate probes (DCFH-DA) (Sigma, USA) dissolved in medium were added into each well at a final concentration of 20  $\mu\text{M}$  and incubated for 30 min at 37 °C. Afterwards, BV2 cells were washed with cold PBS three times and resuspended in PBS, analyzing with flow cytometer (Beckman, USA) at 485 nm for excitation and 530 nm for emission.

#### 4.4.8. DPPH assay

The radical quenching effects of tested compounds and melatonin were evaluated with the DPPH method using serotonin as the standard. Both compounds and positive reference were evaluated at a final concentration of 2.5, 5, 10, 20, 40  $\mu\text{M}$ . In detail, 100  $\mu\text{L}$  of compounds and positive standards diluted in ethanol were mixed with the same volume of 700  $\mu\text{mol}/\text{L}$  ethanol solution of DPPH. The mixed solution was shaken vigorously, and left in dark at room temperature for 30 min. Its absorbance was read using a microplate reader (Bio-Rad Laboratories, CA, USA) at 515 nm. The anti-radical activity was calculated using the following equation:  $[(\text{Abs}_{\text{Control}}/\text{Abs}_{\text{Test}})/\text{Abs}_{\text{Control}}] \times 100\%$ .  $\text{EC}_{50}$  values were calculated by IBM SPSS Statistics 25.0. Data were given as the mean from three independent experiments.

#### 4.4.9. Evaluation on expression of GFAP in LPS-induced C6 cells model and expression of Iba-1 in LPS-induced in BV2 cells

The C6 and BV2 cells in logarithmic growth phase were collected after being dissociated by trypsin, and then seeded on glass slides at a density of  $5 \times 10^5$  cells/mL. After attachment, the cells were

divided into blank control group, LPS treated group and LPS + compound treatment group. In LPS + compound treated group, the final concentration of compounds was 20  $\mu\text{M}$ . In LPS treated group and blank group, equal volume of DMSO was added. At the same time, LPS of 10  $\mu\text{g}/\text{mL}$  and 1  $\mu\text{g}/\text{mL}$  was added to glass slides of C6 and BV2 respectively apart from blank group. After incubation for 24 h, the culture solution was discarded and PBS was used to wash at least three times. Then 50  $\mu\text{L}$  pre-cooled paraformaldehyde (4%) was added to the glass slides and kept for 10 min at room temperature to fix the cells. Next, sealing solution (PBS solution containing 1% BSA and 0.3% Triton x-100) was added and kept for 1 h at room temperature and discarded. In the next stage, glial fibrillary acidic protein antibody (GFAP Ab: Affinity Biosciences, USA, Lot AF6166) and ionized calcium-binding adapter molecule 1 antibody (Iba-1 Ab: Abcam, Cambridge, UK, Lot ab178846) were diluted in sealant (1% BSA and 0.3% Triton x-100) at a 1:100 dilution rate and added dropwise into C6 and BV2 respectively. The glass slides were then incubated overnight in dark at 4 °C. After washing with PBS for three times, secondary antibody was added after diluted with sealant (1% BSA and 0.3% Triton x-100) at a 1:200 dilution rate, and incubated for 2 h in dark at room temperature. In the end, the cover glasses were used to seal the samples after adding anti-fluorescence quenching sealing liquid (containing 2  $\mu\text{g}/\text{mL}$  DAPI). The sealed samples were kept for 5 min in dark at room temperature, and then their images were taken under a confocal laser microscope (Zeiss LSM700, Switzerland). The results were calculated from at least three independent experiments. The immunofluorescence intensity for all groups was measured using Image Pro Plus software. All results were given as the mean  $\pm$  SD; significance between the control groups was determined by analysis of variance (ANOVA), followed by Fisher's PLSD procedure for post hoc comparison which was used to verify the significance between two means. P values of less than 0.05 were considered significant. The data were analyzed by SPSS software.

#### 4.4.10. Animal Experiments

All studies involving animals were performed according to Animal Research: Reporting of In Vivo Experiments (ARRIVE) guidelines, and also had been approved by the Institutional Ethics Committee of Lanzhou University, Gansu, China. Animals were kept and maintained under 12 h light/12 h dark cycle at 25 °C and were fed with food and water ad libitum according to standard rodent procedures.

**4.4.10.1. LPS-induced hippocampal neuroinflammatory model of mice.** Seventy 8-week-old male Kunming mice weighing from 20 g to 25 g were purchased from the GLP Laboratory of Lanzhou University. The mice were divided into seven groups randomly, which were blank group (n = 10), sham operation group (n = 10), model group (n = 10), compound **3** treated group (n = 10), compound **16** treated group (n = 10), melatonin treated group (n = 10), salicylic acid treated group (n = 10). Then LPS injections were built in both model group, melatonin group, salicylic acid group and compounds treated groups, while sham operation group was injected with saline of the same volume. After that, the specific operational procedures were as follows. Firstly, Kunming mice were anaesthetized by intraperitoneal injection with 0.08 mL of chloral hydrate (10%). After exposing the parietal bone, the bregma point could be found according to mouse stereotaxic atlas and regarded as an origin. The location situated 2.00 mm backwards from the origin and 1.00 mm leftwards or rightwards to the sagittal suture was located by a locating pin, where the hippocampus was situated in. Then a small round hole was drilled on the hippocampus with a borehole needle, and an injection needle was lowered by 2–3 mm through the borehole, piercing the lateral ventricle of the mice.

Next, LPS (10 mg/mL; Solarbio, Lot. L8880, China) was slowly injected into the lateral ventricle of mice at a rate of 0.5  $\mu\text{L}/\text{min}$ . In the sham group, 3  $\mu\text{L}$  saline was injected slowly. After the injection, the needle was kept in situ for an additional 5 min and then retrieved slowly from the brain.

After modelling, the mice in compounds, melatonin, salicylic acid treated group were intraperitoneally injected with compounds at a dose of 50 mg/kg (0.08 mL, suspended in saline containing 1% methyl cellulose) per day for six consecutive days, while the mice in model group were injected with saline containing 1% methyl cellulose in the same way. Six days later, the mice were sacrificed to determine the activation of glial cells and the loss of neuronal cell in hippocampus. Six mice of each group (melatonin group, three mice) were firstly perfused with normal saline, followed by 4% paraformaldehyde (PFA) dissolved in 0.1 M sodium phosphate buffer (PBS) (pH = 7.4). The hippocampus was separated out of its cerebral tissues and incubated with 4% paraformaldehyde (PFA) overnight. Then it was stored at a 30% sucrose solution. Next, the hippocampus was cut into thin sections with the thickness of 10  $\mu\text{m}$ . After three times washes with PBS (pH = 7.4) 5 min for each, the thin sections were permeabilized with TritonX-100 (0.3% in TBST) at room temperature, and blocked with 1% bovine serum albumin (BSA) solution for 1 h followed by incubation with a 1:100 dilution of an antibody against glial fibrillary acidic protein (Affinity Biosciences, USA, Lot. AF6166), and a 1:200 dilution of the antibody against ionized calcium-binding adapter protein 1 (Iba-1, Abcam, Cambridge, UK, Lot. ab5076) overnight at 4 °C. Then, the sections were washed with PBS (pH = 7.4) three times, 10 min for each then stained with DAPI staining solution for 10 min at room temperature. Finally, the images were taken under a confocal laser microscope (Zeiss LSM700, Switzerland). The immunofluorescence intensity of images was measured using Image Pro Plus software. Similarly, the hippocampus sections (n = 6) were used for Nissl staining with Methylene Blue (Solarbio, Lot. G1434, China). Finally, the images were taken under a microscope (Motic, China). All results calculated were from six independent samples except for melatonin group, whose result was from three independent samples.

For western blot assay, another four mice of each group were sacrificed. The fresh hippocampi of mice were homogenized in RIPA buffer (Solarbio, R0010, China) containing 1 mM phenylmethanesulfonyl fluoride (PMSF: Solarbio, R0010, China) for 30 min. The protein concentrations were determined by BCA protein assay kit (Solarbio, PC0020, China). Protein samples were run on 12% Tris-glycine SDS-PAGE gels, and blotted with antibodies including glial fibrillary acidic protein antibody (Affinity Biosciences, USA, Lot BF0345) and ionized calcium-binding adapter molecule 1 antibody (Abcam, Cambridge, UK, Lot ab5076). HRP-coupled antibody (Affinity Biosciences, USA) at 1:5000 dilution in blocking buffer for 2 h at room temperature. The immunocomplexes were detected using ECL reagent (Millipore, Billerica, MA) and scanned using the Tanon imaging system (Tanon Science & Technology Co., Ltd, China). All the images were quantified by densitometry using Image J software. All results were given as the mean  $\pm$  SD; Significance between the sham groups was determined by analysis of variance (ANOVA), followed by Fisher's PLSD procedure for post hoc comparison which was used to verify the significance between two means. P values of less than 0.05 were considered significant. The data were analyzed by SPSS software. All results calculated were from four independent samples except for melatonin group, whose result was from three independent samples.

**4.4.10.2. Acute toxicity study.** Acute toxicity studies were carried out according to OECD guidelines. Briefly, thirty 8-week-old

Kunming mice weighing from 20 g to 25 g were purchased from the GLP Laboratory of Lanzhou University. The mice were divided into three groups randomly ( $n = 10$ , five female and five male mice). The first group was treated with saline containing 1% methyl cellulose, the second group was treated with compound **3** at a dose of 1000 mg/kg (suspended in saline containing 1% methyl cellulose), the third group was treated with compound **16** at a dose of 1000 mg/kg (suspended in saline containing 1% methyl cellulose). All treatments were operated by gavage with a single dose. The treated animals were observed continuously for the first 4 h followed by periodic monitoring for another 20 h. Then animals were observed once daily for a period of 14 days. After 14 days, all animals were sacrificed to conduct histological studies on liver, kidney, heart, and stomach by using H and E staining method.

**4.4.10.3. Pharmacokinetics study.** Eighteen 8-week-old male SD rats weighing from 250 g to 280 g were purchased from the GLP Laboratory of Lanzhou University. The rats were randomly distributed into three groups ( $n = 6$ ). The rats were deprived of water and fasted overnight prior to treatment. Melatonin, compounds **3**, **16** were injected intraperitoneally at a dose of 50 mg/kg. After single administration of compounds **3** and **16**, plasma samples were collected from the orbital venous plexus at the following time points: 5 min, 15 min, 45 min, 1 h, 3 h, 5 h, 8 h, 10 h, 24 h for compound **3**; 15 min, 45 min, 1 h, 1.5 h, 3 h, 5 h, 7 h, 9 h, 11 h, 24 h for compound **16**; 5 min, 30 min, 1 h, 2.5 h, 3.5 h for melatonin. Every blood samples were collected in heparinized tubes followed by separating with centrifugation (2500 rpm, 6 min, 4 °C). Then the plasma fraction was separated and stored at  $-80$  °C for LC-MS analysis. For plasma sample preparation, 100  $\mu$ L of samples were accurately measured into each new centrifugal tube and mixed thoroughly by vortex for 30 s. Then, methanol was added to each plasma sample and mixed thoroughly. After centrifugation at 16000 rpm for 10 min at 4 °C, the supernatant of each sample was precisely transferred to an evaporator tube, and dried in nitrogen flow. After drying, the residue was redissolved in methanol, and then analyzed after filtered by filter membrane of 0.22  $\mu$ m. For liquid chromatography and mass spectrometry conditions, chromatographic analyses were performed with a column: Eclipse Plus C18 ( $4.6 \times 150$  mm, 4  $\mu$ m). The HPLC mobile phases consisted of water (0.1% formic acid) (A) and methanol (B). A gradient program was used for the HPLC separation at 0.5 mL/min. Chromatographic conditions: Mobile phase: 0–7 min, MeOH: H<sub>2</sub>O = 20:80; 7–16 min MeOH:H<sub>2</sub>O = 95:5, 16–25 min, MeOH:H<sub>2</sub>O = 20:80; Wavelength: 254 nm; Column temperature: 25 °C. The column eluent was directly introduced into ES-API (Agilent InfinityLab LC/MSD; USA). Finally, the obtained data were processed by Pksolver2.0. The results were calculated from the mean of six independent experiments.

#### 4.5. Statistical analysis

All results are given as the mean  $\pm$  SD; significance between the groups was determined by analysis of variance (ANOVA), followed by Fisher's PLSD procedure for post hoc comparison, to verify the significance between two means. P values of less than 0.05 were considered significant. The data were analyzed by SPSS software.

#### Declaration of competing interest

The authors declare that they have no known competing financial interests or personal relationships that could have appeared to influence the work reported in this paper.

#### Acknowledgements

This work is dedicated to Lanzhou University on the occasion of its 110th birthday. It was financially supported by the Recruitment Program of Global Experts (1000 Talents Plan), and the Fundamental Research Funds for the Central Universities (lzujbky-2019-ct08).

#### Appendix A. Supplementary data

Supplementary data to this article can be found online at <https://doi.org/10.1016/j.ejmech.2020.112217>.

#### Abbreviations

IC <sub>50</sub>	half-maximum inhibitory concentration
COX-2	Cyclooxygenase-2
COX-1	Cyclooxygenase-1
LPS	lipopolysaccharide
CNS	Central nervous system
PBS	Phosphate-buffered saline
NO	nitric oxide
TNF- $\alpha$	Tumor necrosis factor-alpha
IL-10	Interleukin-10
PGE <sub>2</sub>	prostaglandin E <sub>2</sub>
iNOS	Inducible nitric oxide synthase
CA1	Cornu Ammonis
SD	Standard deviation
i.p	Intraperitoneally
Iba-1	Ionized calcium-binding adapter molecule 1
GFAP	Glial fibrillary acidic protein
AD	Alzheimer's disease
ROS	reactive oxygen species
DCFH-DA	2',7'-dichlorodi-hydrofluorescein
DMSO	dimethyl sulphoxide
FBS	fetal bovine serum
LD <sub>50</sub>	dose that is lethal in 50% of test subjects
M	multiplet (spectral)
HOBt	1-Hydroxybenzotriazole

#### References

- [1] W.W. Chen, X. Zhang, W.J. Huang, Role of neuroinflammation in neurodegenerative diseases, *Mol. Med. Rep.* 13 (2016) 3391–3396, <https://doi.org/10.3892/mmr.2016.4948>.
- [2] E. Czirri, T. Wyss-Coray, The immunology of neurodegeneration, *J. Clin. Invest.* 122 (2012) 1156–1163, <https://doi.org/10.1172/jci58656>.
- [3] K. Yao, H.B. Zu, Microglial polarization: novel therapeutic mechanism against Alzheimer's disease, *Inflammopharmacology* 28 (2020) 95–110, <https://doi.org/10.1007/s10787-019-00613-5>.
- [4] L. Xu, D. He, Y. Bai, Microglia-mediated inflammation and neurodegenerative disease, *Mol. Neurobiol.* 53 (2016) 6709–6715, <https://doi.org/10.1007/s12035-015-9593-4>.
- [5] S. Piirainen, A. Youssef, C. Song, A.V. Kalueff, G.E. Landreth, T. Malm, L. Tian, Psychosocial stress on neuroinflammation and cognitive dysfunctions in Alzheimer's disease: the emerging role for microglia? *Neurosci. Biobehav. Rev.* 77 (2017) 148–164, <https://doi.org/10.1016/j.neubiorev.2017.01.046>.
- [6] W.J. Streit, Microglia as neuroprotective, immunocompetent cells of the CNS, *Glia* 40 (2002) 133–139, <https://doi.org/10.1002/glia.10154>.
- [7] M.S. Uddin, M.T. Kabir, A. Al Mamun, M.M. Abdel-Daim, G.E. Barreto, G.M. Ashraf, APOE and Alzheimer's disease: evidence mounts that targeting APOE4 may combat Alzheimer's pathogenesis, *Mol. Neurobiol.* 56 (2019) 2450–2465, <https://doi.org/10.1007/s12035-018-1237-z>.
- [8] X. Wang, G. Sun, T. Feng, J. Zhang, X. Huang, T. Wang, Z. Xie, X. Chu, J. Yang, H. Wang, S. Chang, Y. Gong, L. Ruan, G. Zhang, S. Yan, W. Lian, C. Du, D. Yang, Q. Zhang, F. Lin, J. Liu, H. Zhang, C. Ge, S. Xiao, J. Ding, M. Geng, Sodium oligomannate therapeutically remodels gut microbiota and suppresses gut bacterial amino acids-shaped neuroinflammation to inhibit Alzheimer's disease progression, *Cell Res.* 29 (2019) 787–803, <https://doi.org/10.1038/s41422-019-0216-x>.
- [9] I.B. Hovens, R.G. Schoemaker, E.A. van der Zee, A.R. Absalom, E. Heineman, B.L. van Leeuwen, Postoperative cognitive dysfunction: involvement of

- neuroinflammation and neuronal functioning, *Brain Behav. Immun.* 38 (2014) 202–210, <https://doi.org/10.1016/j.bbi.2014.02.002>.
- [10] Z.L. Liu, J. Zhang, A. Zhang, Design of Multivalent ligand targeting g-protein-coupled receptors, *Curr. Pharmaceut. Des.* 15 (2009) 682–718, <https://doi.org/10.2174/138161209787315639>.
- [11] S.A. Shah, M. Khan, M.H. Jo, M.G. Jo, F.U. Amin, M.O. Kim, Melatonin stimulates the SIRT1/Nrf 2 signaling pathway counteracting lipopolysaccharide (LPS)-induced oxidative stress to rescue postnatal rat brain, *CNS Neurosci. Ther.* 23 (2017) 33–44, <https://doi.org/10.1111/cns.12588>.
- [12] E. Park, H.S. Chun, Melatonin attenuates manganese and lipopolysaccharide-induced inflammatory activation of BV2 microglia, *Neurochem. Res.* 42 (2017) 656–666, <https://doi.org/10.1007/s11064-016-2122-7>.
- [13] R. Niranjani, C. Nath, R. Shukla, Melatonin attenuated mediators of neuroinflammation and alpha-7 nicotinic acetylcholine receptor mRNA expression in lipopolysaccharide (LPS) stimulated rat astrocytoma cells, *C6, Free Radic. Res.* 46 (2012) 1167–1177, <https://doi.org/10.3109/10715762.2012.697626>.
- [14] E. Tyagi, R. Agrawal, C. Nath, R. Shukla, Effect of melatonin on neuroinflammation and acetylcholinesterase activity induced by LPS in rat brain, *Eur. J. Pharmacol.* 640 (2010) 206–210, <https://doi.org/10.1016/j.ejphar.2010.04.041>.
- [15] L.P.H. Andersen, I. Gogenur, J. Rosenberg, R.J. Reiter, The safety of melatonin in humans, *Clin. Drug Invest.* 36 (2016) 169–175, <https://doi.org/10.1007/s40261-015-0368-5>.
- [16] E. Ramos, J. Egea, C. de los Rios, J. Marco-Contelles, A. Romero, Melatonin as a versatile molecule to design novel multitarget hybrids against neurodegeneration, *Future Med. Chem.* 9 (2017) 765–780, <https://doi.org/10.4155/fmc-2017-0014>.
- [17] A. Menendezpelaez, R.J. Reiter, Distribution of melatonin in mammalian-tissues - the relative importance of nuclear versus cytosolic localization, *J. Pineal Res.* 15 (1993) 59–69, <https://doi.org/10.1111/j.1600-079X.1993.tb00511.x>.
- [18] K. Yeleswaram, L.G. McLaughlin, J.O. Knipe, D. Schabdach, Pharmacokinetics and oral bioavailability of exogenous melatonin in preclinical animal models and clinical implications, *J. Pineal Res.* 22 (1997) 45–51, <https://doi.org/10.1111/j.1600-079X.1997.tb00302.x>.
- [19] S. Rivara, D. Pala, A. Bedini, G. Spadoni, Therapeutic uses of melatonin and melatonin derivatives: a patent review (2012–2014), *Expert Opin. Ther. Pat.* 25 (2015) 425–441, <https://doi.org/10.1517/13543776.2014.1001739>.
- [20] P.L. McGeer, E.G. McGeer, NSAIDs and Alzheimer disease: epidemiological, animal model and clinical studies, *Neurobiol. Aging* 28 (2007) 639–647, <https://doi.org/10.1016/j.neurobiolaging.2006.03.013>.
- [21] S.C. Vlad, D.R. Miller, N.W. Kowall, D.T. Felson, Protective effects of NSAIDs on the development of Alzheimer disease, *Neurology* 70 (2008) 1672–1677, <https://doi.org/10.1212/01.wnl.0000311269.57716.63>.
- [22] J.M. Janjic, K. Vasudeva, M. Saleem, A. Stevens, L. Liu, S. Patel, J.A. Pollock, Low-dose NSAIDs reduce pain via macrophage targeted nanoemulsion delivery to neuroinflammation of the sciatic nerve in rat, *J. Neuroimmunol.* 318 (2018) 72–79, <https://doi.org/10.1016/j.jneuroim.2018.02.010>.
- [23] X. Lan, R. Liu, L. Sun, T.T. Zhang, G.H. Du, Methyl salicylate 2-O-beta-(D)-lactoside, a novel salicylic acid analogue, acts as an anti-inflammatory agent on microglia and astrocytes, *J. Neuroinflammation* 8 (2011) 7, <https://doi.org/10.1186/1742-2094-8-98>.
- [24] B. Thrash-Williams, S.S. Karuppagounder, D. Bhattacharya, M. Ahuja, V. Suppiramaniam, M. Dhanasekaran, Methamphetamine-induced dopaminergic toxicity prevented owing to the neuroprotective effects of salicylic acid, *Life Sci.* 154 (2016) 24–29, <https://doi.org/10.1016/j.lfs.2016.02.072>.
- [25] I.R.A. Mackenzie, D.G. Munoz, Nonsteroidal anti-inflammatory drug use and Alzheimer-type pathology in aging, *Neurology* 50 (1998) 986–990, <https://doi.org/10.1212/wnl.50.4.986>.
- [26] I.R.A. Mackenzie, Anti-inflammatory drugs and Alzheimer-type pathology in aging, *Neurology* 54 (2000) 732–734, <https://doi.org/10.1212/wnl.54.3.732>.
- [27] M.A.A. Blom, M.G.H. van Twillert, S.C. de Vries, F. Engels, C.E. Finch, R. Veerhuis, P. Eikelenboom, NSAIDs inhibit the IL-1 beta-induced IL-6 release from human post-mortem astrocytes: the involvement of prostaglandin E-2, *Brain Res.* 777 (1997) 210–218, [https://doi.org/10.1016/s0006-8993\(97\)01204-3](https://doi.org/10.1016/s0006-8993(97)01204-3).
- [28] S. Aid, F. Bosetti, Targeting cyclooxygenases-1 and-2 in neuroinflammation: therapeutic implications, *Biochimie* 93 (2011) 46–51, <https://doi.org/10.1016/j.biochi.2010.09.009>.
- [29] E.D. Alfadly, P.A. Elzahhar, A. Tramarin, S. Elkazaz, H. Shaltout, M.M. Abu-Serie, J. Janockova, O. Soukup, D.A. Ghareeb, A.F. El-Yazbi, R.W. Rafah, N.-M.Z. Bakkar, F. Kobeissy, I. Iriepa, I. Moraleda, M.N.S. Saudi, M. Bartolini, A.S.F. Belal, Tackling neuroinflammation and cholinergic deficit in Alzheimer's disease: multi-target inhibitors of cholinesterases, cyclooxygenase-2 and 15-lipoxygenase, *Eur. J. Med. Chem.* 167 (2019) 161–186, <https://doi.org/10.1016/j.ejmech.2019.02.012>.
- [30] S.-H. Choi, S. Aid, L. Caracciolo, S.S. Minami, T. Niikura, Y. Matsuoka, R.S. Turner, M.P. Mattson, F. Bosetti, Cyclooxygenase-1 inhibition reduces amyloid pathology and improves memory deficits in a mouse model of Alzheimer's disease, *J. Neurochem.* 124 (2013) 59–68, <https://doi.org/10.1111/jnc.12059>.
- [31] A.S. Cornec, L. Monti, J. Kovalevich, V. Makani, M.J. James, K.G. Vijayendran, K. Oukoloff, Y.M. Yao, V.M.Y. Lee, J.Q. Trojanowski, A.B. Smith, K.R. Brunden, C. Ballatore, Multitargeted imidazoles: potential therapeutic leads for Alzheimer's and other neurodegenerative diseases, *J. Med. Chem.* 60 (2017) 5120–5145, <https://doi.org/10.1021/acs.jmedchem.7b00475>.
- [32] A. Arfi, M. Richard, C. Gandolphe, D. Bonnefont-Rousselot, P. Therond, D. Scherman, Neuroinflammatory and oxidative stress phenomena in MPS IIIA mouse model: the positive effect of long-term aspirin treatment, *Mol. Genet. Metabol.* 103 (2011) 18–25, <https://doi.org/10.1016/j.ymgme.2011.01.015>.
- [33] Y.P. Wang, Y. Wu, L.Y. Li, J. Zheng, R.G. Liu, J.P. Zhou, S.Y. Yuan, Y. Shang, S.L. Yao, Aspirin-triggered lipoxin A(4) attenuates LPS-induced pro-inflammatory responses by inhibiting activation of NF-kappa B and MAPKs in BV-2 microglial cells, *J. Neuroinflammation* 8 (2011) 12, <https://doi.org/10.1186/1742-2094-8-95>.
- [34] C.Y. Yao, D. Yang, Z.Z. Wan, Z.X. Wang, R.G. Liu, Y. Wu, S.L. Yao, S.Y. Yuan, Y. Shang, Aspirin-triggered lipoxin A(4) attenuates lipopolysaccharide induced inflammatory response in primary astrocytes, *Int. Immunopharm.* 18 (2014) 85–89, <https://doi.org/10.1016/j.intimp.2013.10.028>.
- [35] R. Calvello, M.A. Panaro, M.L. Carbone, A. Cianciulli, M.G. Perrone, P. Vitale, P. Malerba, A. Scilimati, Novel selective COX-1 inhibitors suppress neuro-inflammatory mediators in LPS-stimulated N13 microglial cells, *Pharmacol. Res.* 65 (2012) 137–148, <https://doi.org/10.1016/j.phrs.2011.09.009>.
- [36] X. Jin, M.Y. Liu, D.F. Zhang, X. Zhong, K. Du, P. Qian, H. Rao, M.J. Wei, Natural products as a potential modulator of microglial polarization in neurodegenerative diseases, *Pharmacol. Res.* 145 (2019) 28, <https://doi.org/10.1016/j.phrs.2019.104253>.
- [37] J.M. Rubio-Perez, J.M. Morillas-Ruiz, A Review: inflammatory process in Alzheimer's disease, role of cytokines, *Sci. World J.* 15 (2012), <https://doi.org/10.1100/2012/756357>.
- [38] F.A. Oliveira, R.N. de Almeida, M.D. Sousa, J.M. Barbosa, S.A. Diniz, I.A. de Medeiros, Anticonvulsant properties of N-salicyloyltryptamine in mice, *Pharmacol., Biochem. Behav.* 68 (2001) 199–202, [https://doi.org/10.1016/s0091-3057\(00\)00484-6](https://doi.org/10.1016/s0091-3057(00)00484-6).
- [39] J. Gasparotto, M.A. de Bittencourt Pasquali, N. Somensi, L.M. Vasques, J.C. Fonseca Moreira, R.N. de Almeida, J.M. Barbosa-Filho, M.d.F. Vanderlei de Souza, S.J. Chavez Gutierrez, L.J. Quintans Junior, D.P. Gelain, Effect of N-salicyloyltryptamine (STP), a novel tryptamine analogue, on parameters of cell viability, oxidative stress, and immunomodulation in RAW 264.7 macrophages, *Cell Biol. Toxicol.* 29 (2013) 175–187, <https://doi.org/10.1007/s10565-013-9245-2>.
- [40] D.A.M. Araujo, R.A. Mafra, A.L.P. Rodrigues, V. Miguel-Silva, P.S.L. Beirao, R.N. de Almeida, L. Quintans, M.F.V. de Souza, J.S. Cruz, N-Salicyloyltryptamine, a new anticonvulsant drug, acts on voltage-dependent Na<sup>+</sup>, Ca<sup>2+</sup>, and K<sup>+</sup> ion channels, *Br. J. Pharmacol.* 140 (2003) 1331–1339, <https://doi.org/10.1038/sj.bjp.0705471>.
- [41] L.J. Quintans-Junior, D.A. Silva, J.S. Siqueira, A.A.S. Araujo, R.S.S. Barreto, L.R. Bonjardim, J.M. DeSantana, W. De Lucca Junior, M.F.V. Souza, S.J.C. Gutierrez, J.M. Barbosa-Filho, V.J. Santana-Filho, D.A.M. Araujo, R.N. Almeida, Bioassay-guided evaluation of antinociceptive effect of N-salicyloyltryptamine: a behavioral and electrophysiological approach, *J. Biomed. Biotechnol.* (2010), <https://doi.org/10.1155/2010/230745>.
- [42] B.P. Sousa-Neto, B.S. Gomes, F.V.M. Cunha, D.D.R. Arcanjo, S.J.C. Gutierrez, M.F.V. Souza, F.R.C. Almeida, F.A. Oliveira, Antiedematogenic activity of the indole derivative N-salicyloyltryptamine in animal models, *An. Acad. Bras. Cienc.* 90 (2018) 185–194, <https://doi.org/10.1590/0001-3765201720160502>.
- [43] L.J. Quintans-Junior, D.A. Silva, J.S. Siqueira, A.A.S. Araújo, A.G. Guimarães, R.A.N. Araújo, D.A.M. Araújo, M.d.F.V. Souza, S.J.C. Gutierrez, J.M. Barbosa-Filho, R.N. Almeida, Anticonvulsant property of N-salicyloyltryptamine: evidence of enhance of central GABAergic neurotransmission, *J. Epilepsy Clin. Neurophysiol.* 15 (2009) 165–168, <https://doi.org/10.1590/s1676-26492009000400005>.
- [44] T.M. Rose, C.A. Reilly, C.E. Deering-Rice, C. Brewster, C. Brewster, Inhibition of FAAH, TRPV1, and COX2 by NSAID-serotonin conjugates, *Bioorg. Med. Chem. Lett.* 24 (2014) 5695–5698, <https://doi.org/10.1016/j.bmlc.2014.10.064>.
- [45] C.L. Fleming, T.D. Ashton, V. Gaur, S.L. McGee, F.M. Pfeffer, Improved synthesis and structural reassignment of MC1568: a class IIa selective HDAC inhibitor, *J. Med. Chem.* 57 (2014) 1132–1135, <https://doi.org/10.1021/jm401945k>.
- [46] J.D. Deng, S. Lei, Y. Jiang, H.H. Zhang, X.L. Hu, H.X. Wen, W. Tan, Z. Wang, A concise synthesis and biological study of evodiamine and its analogues, *Chem. Commun.* 55 (2019) 3089–3092, <https://doi.org/10.1039/c9cc00434c>.
- [47] Y.Z. Li, T.T. Feng, P. Liu, C. Liu, X. Wang, D.S. Li, N. Li, M.H. Chen, Y.N. Xu, S.Y. Si, Optimization of rutaecarpine as ABCA1 up-regulator for treating atherosclerosis, *ACS Med. Chem. Lett.* 5 (2014) 884–888, <https://doi.org/10.1021/ml500131a>.
- [48] N. Zhao, Z.-L. Li, D.-H. Li, Y.-T. Sun, D.-T. Shan, J. Bai, Y.-H. Pei, Y.-K. Jing, H.-M. Hua, Quinolone and indole alkaloids from the fruits of *Euodia rutaecarpa* and their cytotoxicity against two human cancer cell lines, *Phytochemistry* 109 (2015) 133–139, <https://doi.org/10.1016/j.phytochem.2014.10.020>.
- [49] F. Pandolfi, F. D'Acerno, M. Bortolami, D. De Vita, F. Gallo, A. De Meo, R. Di Santo, R. Costi, G. Simonetti, L. Scipione, Searching for new agents active against *Candida albicans* biofilm: a series of indole derivatives, design, synthesis and biological evaluation, *Eur. J. Med. Chem.* 165 (2019) 93–106, <https://doi.org/10.1016/j.ejmech.2019.01.012>.
- [50] G. Tang, R. Xiong, X. Deng, D. He, X. Lei, Indole Amide Compounds for Selective Inhibition of Gastric Cancer Cell Line MGC-803, 2018. Patent CN 108530337A, China.
- [51] G. Tang, R. Xiong, X. Deng, D. He, X. Lei, Indole Amide Compounds for Cancer, 2018. Patent CN 108623511A, China.
- [52] R. Cabezas, E. Baez-Jurado, O. Hidalgo-Lanussa, V. Echeverria, G.M. Ashraf,

- A. Sahebkar, G.E. Barreto, Growth factors and neuroglobin in astrocyte protection against neurodegeneration and oxidative stress (vol 56, pg 2339, *Mol. Neurobiol.* 56 (2019) (2019), <https://doi.org/10.1007/s12035-018-1257-8>, 2352–2352.
- [53] F. Denizot, R. Lang, Rapid colorimetric assay for cell-growth and survival - modifications to the tetrazolium dye procedure giving improved sensitivity and reliability, *J. Immunol. Methods* 89 (1986) 271–277, [https://doi.org/10.1016/0022-1759\(86\)90368-6](https://doi.org/10.1016/0022-1759(86)90368-6).
- [54] G.C. Brown, V. Borutaite, Nitric oxide inhibition of mitochondrial respiration and its role in cell death, *Free Radical Biol. Med.* 33 (2002) 1440–1450, [https://doi.org/10.1016/s0891-5849\(02\)01112-7](https://doi.org/10.1016/s0891-5849(02)01112-7).
- [55] P. Mander, G.C. Brown, Activation of microglial NADPH oxidase is synergistic with glial iNOS expression in inducing neuronal death: a dual-key mechanism of inflammatory neurodegeneration, *J. Neuroinflammation* 2 (2005) 15, <https://doi.org/10.1186/1742-2094-2-20>.
- [56] S. Sorce, M. Nuvolone, A. Keller, J. Falsig, A. Varol, P. Schwarz, M. Bieri, H. Budka, A. Aguzzi, The role of the NADPH oxidase NOX2 in prion pathogenesis, *PLoS Pathog.* 10 (2014) 12, <https://doi.org/10.1371/journal.ppat.1004531>.
- [57] N.S. Bryan, M.B. Grisham, Methods to detect nitric oxide and its metabolites in biological samples, *Free Radical Biol. Med.* 43 (2007) 645–657, <https://doi.org/10.1016/j.freeradbiomed.2007.04.026>.
- [58] T.T. Tang, T. Gong, W. Jjiang, R.B. Zhou, GPCRs in NLRP3 inflammasome activation, regulation, and therapeutics, *Trends Pharmacol. Sci.* 39 (2018) 798–811, <https://doi.org/10.1016/j.tips.2018.07.002>.
- [59] M.E. Lull, M.L. Block, Microglial activation and chronic neurodegeneration, *Neurotherapeutics* 7 (2010) 354–365, <https://doi.org/10.1016/j.nurt.2010.05.014>.
- [60] M.L. Block, J.S. Hong, Microglia and inflammation-mediated neurodegeneration: multiple triggers with a common mechanism, *Prog. Neurobiol.* 76 (2005) 77–98, <https://doi.org/10.1016/j.pneurobio.2005.06.004>.
- [61] L. Minghetti, Cyclooxygenase-2 (COX-2) in inflammatory and degenerative brain diseases, *J. Neuropathol. Exp. Neurol.* 63 (2004) 901–910, <https://doi.org/10.1093/jnen/63.9.901>.
- [62] E. Molina-Holgado, J.M. Vela, A. Arevalo-Martin, C. Guaza, LPS/IFN-gamma cytotoxicity in oligodendroglial cells: role of nitric oxide and protection by the anti-inflammatory cytokine IL-10, *Eur. J. Neurosci.* 13 (2001) 493–502, <https://doi.org/10.1046/j.0953-816x.2000.01412.x>.
- [63] K. Strle, J.H. Zhou, S.R. Broussard, H.D. Venters, R.W. Johnson, G.G. Freund, R. Dantzer, K.W. Kelley, IL-10 promotes survival of microglia without activating Akt, *J. Neuroimmunol.* 122 (2002) 9–19, [https://doi.org/10.1016/s0165-5728\(01\)00444-1](https://doi.org/10.1016/s0165-5728(01)00444-1).
- [64] R. Barhourni, J. Faske, X.H. Liu, R.B. Tjalkens, Manganese potentiates lipopolysaccharide-induced expression of NOS2 in C6 glioma cells through mitochondrial-dependent activation of nuclear factor kappaB, *Mol. Brain Res.* 122 (2004) 167–179, <https://doi.org/10.1016/j.molbrainres.2003.12.009>.
- [65] J.U. Johansson, N.S. Woodling, J. Shi, K.I. Andreasson, Inflammatory cyclooxygenase activity and PGE2 signaling in models of Alzheimer's disease, *Curr. Immunol. Rev.* 11 (2015) 125–131, <https://doi.org/10.2174/1573395511666150707181414>.
- [66] Nathaniel.S. Woodling, Katrin I. Andreasson, Toxic and protective effects of neuroinflammation and PGE2 signaling in Alzheimer's disease, *ACS Chem. Neurosci.* (2016), <https://doi.org/10.1021/acschemneuro.6b00016>.
- [67] X. Liang, L. Wu, Q. Wang, T. Hand, M. Bilak, L. McCullough, K. Andreasson, Function of COX-2 and prostaglandins in neurological disease, *J. Mol. Neurosci.* 33 (2007) 94–99, <https://doi.org/10.1007/s12031-007-0058-8>.
- [68] E.F. Shevtsova, D.V. Vinogradova, M.E. Neganova, M. Avila-Rodriguez, G.M. Ashraf, G.E. Barreto, S.O. Bachurin, G. Aliev, Mitochondrial permeability transition pore as a suitable target for neuroprotective agents against Alzheimer's disease, *CNS Neurol. Disord. - Drug Targets* 16 (2017) 677–685, <https://doi.org/10.2174/1871527316666170424114444>.
- [69] A. Alexiou, G. Soursoy, S. Chatzichronis, E. Gasparatos, M.A. Kamal, N.S. Yarla, A. Perveen, G.E. Barreto, G.M. Ashraf, Role of GTPases in the regulation of mitochondrial dynamics in Alzheimer's disease and CNS-related disorders, *Mol. Neurobiol.* 56 (2019) 4530–4538, <https://doi.org/10.1007/s12035-018-1397-x>.
- [70] A. Roy, A. Jana, K. Yatish, M.B. Freidt, Y.K. Fung, J.A. Martinson, K. Pahan, Reactive oxygen species up-regulate CD11b in microglia via nitric oxide: implications for neurodegenerative diseases, *Free Radic. Biol. Med.* 45 (2008) 686–699, <https://doi.org/10.1016/j.freeradbiomed.2008.05.026>.
- [71] D.X. Liu, J. Wen, J. Liu, L.P. Li, The roles of free radicals in amyotrophic lateral sclerosis: reactive oxygen species and elevated oxidation of protein, DNA, and membrane phospholipids, *Faseb. J.* 13 (1999) 2318–2328, <https://doi.org/10.1096/fasebj.13.15.2318>.
- [72] S.B. Kedare, R.P. Singh, Genesis and development of DPPH method of anti-oxidant assay, *J. Food Sci. Technol.-Mysore.* 48 (2011) 412–422, <https://doi.org/10.1007/s13197-011-0251-1>.
- [73] V. Henry, V. Paille, F. Lelan, P. Brachet, P. Damier, Kinetics of microglial activation and degeneration of dopamine-containing neurons in a rat model of Parkinson disease induced by 6-Hydroxydopamine, *J. Neuropathol. Exp. Neurol.* 68 (2009) 1092–1102, <https://doi.org/10.1097/NEN.0b013e3181b767b4>.
- [74] H. Zhou, Z. Liu, J. Liu, J. Wang, D. Zhou, Z. Zhao, S. Xiao, E. Tao, W.Z. Suo, Fractionated radiation-induced acute encephalopathy in a young rat model: cognitive dysfunction and histologic findings, *Am. J. Neuroradiol.* 32 (2011) 1795–1800, <https://doi.org/10.3174/ajnr.A2643>.
- [75] S. Tanaka, M. Ide, T. Shibutani, H. Ohtaki, S. Numazawa, S. Shioda, T. Yoshida, Lipopolysaccharide-induced microglial activation induces learning and memory deficits without neuronal cell death in rats, *J. Neurosci. Res.* 83 (2006) 557–566, <https://doi.org/10.1002/jnr.20752>.
- [76] E. Tyagi, R. Agrawal, C. Nath, R. Shukla, Influence of LPS-induced neuroinflammation on acetylcholinesterase activity in rat brain, *J. Neuroimmunol.* 205 (2008) 51–56, <https://doi.org/10.1016/j.jneuroim.2008.08.015>.
- [77] B.J. Holliman, P.A. Chyka, Problems in assessment of acute melatonin overdose, *South. Med. J.* 90 (1997) 451–453, <https://doi.org/10.1097/00007611-199704000-00020>.
- [78] A.L. Morera, M. Henry, M. De la Varga, Safety in melatonin use, *Actas Esp. Psiquiatr.* 29 (2001) 334–337.
- [79] H.E. Johnson, J.M. Dotson, C.S. Ellis, K.K. Hill, Severe hypotension in an adolescent after a melatonin overdose, *J. Child Adolesc. Psychopharmacol.* 29 (2019) 726–727, <https://doi.org/10.1089/cap.2019.0108>.
- [80] S. Shao, R. Marino, A. Scoccamarro, M. Abesamis, Lytes out: massive melatonin overdose with resulting profound hyponatremia, *Clin. Toxicol.* 57 (2019), 921–921.
- [81] Oecd, Test No. 425: Acute Oral Toxicity: Up-And-Down Procedure (UDP), OECD, 2008, pp. 1–27, <https://doi.org/10.1787/9789264071049-en>.